Additive manufacturing of bioactive glass biomaterials

Methods 208 (2022) 75–91

Contents lists available at ScienceDirect

Methods

journal homepage: www.elsevier.com/locate/ymeth

Additive manufacturing of bioactive glass biomaterials

Sara Simorgh [a,b,1], Neda Alasvand [b,c,1], Mahboobe Khodadadi [c], Faezeh Ghobadi [d], Maziar Malekzadeh Kebria [b], Peiman Brouki Milan [a,b], Saeid Kargozar [e], Francesco Baino [f], Ali Mobasheri [g,h,i,j], Masoud Mozafari [g,*]

[a] Cellular and Molecular Research Centre, Iran University of Medical Sciences, Tehran, Iran
[b] Department of Tissue Engineering and Regenerative Medicine, Faculty of Advanced Technologies in Medicine, Iran University of Medical Sciences, Tehran, Iran
[c] Department of Nanotechnology and Advanced Materials, Materials and Energy Research Center (MERC), Tehran, Iran
[d] Department of Chemical and Petroleum Engineering, Sharif University of Technology, Tehran, Iran
[e] Tissue Engineering Research Group (TERG), Department of Anatomy and Cell Biology, School of Medicine, Mashhad University of Medical Sciences, Mashhad, Iran
[f] Institute of Materials Physics and Engineering, Department of Applied Science and Technology (DISAT), Politecnico di Torino, Corso Duca degli Abruzzi 24, 10129 Torino, Italy
[g] Research Unit of Health Sciences and Technology, Faculty of Medicine, University of Oulu, Oulu, Finland
[h] Department of Regenerative Medicine, State Research Institute Centre for Innovative Medicine, Vilnius, Lithuania
[i] Department of Joint Surgery, First Affiliated Hospital of Sun Yat-sen University, Guangzhou, China
[j] World Health Organization Collaborating Centre for Public Health Aspects of Musculoskeletal Health and Aging, Liege, Belgium

ARTICLE INFO

Keywords:
Additive manufacturing
3D printing, Bioprinting, Bioactive glasses
Bioinks
Biomaterials
Tissue engineering

ABSTRACT

Tissue engineering (TE) and regenerative medicine have held great promises for the repair and regeneration of damaged tissues and organs. Additive manufacturing has recently appeared as a versatile technology in TE strategies that enables the production of objects through layered printing. By applying 3D printing and bioprinting, it is now possible to make tissue-engineered constructs according to desired thickness, shape, and size that resemble the native structure of lost tissues. Up to now, several organic and inorganic materials were used as raw materials for 3D printing; bioactive glasses (BGs) are among the most hopeful substances regarding their excellent properties (e.g., bioactivity and biocompatibility). In addition, the reported studies have confirmed that BG-reinforced constructs can improve osteogenic, angiogenic, and antibacterial activities. This review aims to provide an up-to-date report on the development of BG-containing raw biomaterials that are currently being employed for the fabrication of 3D printed scaffolds used in tissue regeneration applications with a focus on their advantages and remaining challenges.

1. Introduction

Tissue-engineered (TE) constructs have gradually achieved a substantial place in the research field; suitable biocompatible substances can be used as raw materials for fabricating pre-designed structures with diverse shapes and sizes. Accordingly, it seems feasible to generate the construction of complex systems that can mimic the natural architecture of human tissues.

Up to now, a huge number of grafts (e.g., bone, cartilage, skin, etc.) were successfully implanted into patients; however, most of the applied approaches have been extremely expensive [1]. Tissue engineering (TE) still plays a moderately small role in providing complex tissues and organs for transplantation, despite its huge potential. One of the main goals in tissue engineering is to fabricate biodegradable scaffolds with a high regenerative capability and suitable mechanical properties [2,3]. Additionally, tissue-engineered constructs should have an appropriate porous structure and an acceptable pore size for cell migration and the exchange of wastes and nutrients, among other requirements. [4–6]. The conventional fabrication approaches (e.g., polymeric sponge replication) generally do not provide satisfactory control over the architecture of scaffolds (shape, pore size, pore network, etc.).

Additive manufacturing, which is also simply known as three-dimensional (3D) printing, has grown over the last 30 years, and its use has impressively accelerated during the last 5 years [7]. This approach is a material-oriented manufacturing technology and there is a

* Corresponding author.
E-mail address: mozafari.masoud@gmail.com (M. Mozafari).
[1] These authors contributed equally to this work.

https://doi.org/10.1016/j.ymeth.2022.10.010
Received 27 July 2022; Received in revised form 22 October 2022; Accepted 27 October 2022
Available online 2 November 2022

Nomenclature

Tissue engineering (TE)
Three-dimensional (3D)
Bioactive glasses (BGs)
Copper (Cu)
Cobalt (Co)
Magnesium (Mg)
Silver (Ag)
Zinc (Zn)
Strontium (Sr)
Computer-aided manufacturing (CAM)
Computer-assisted design (CAD)
Magnetic resonance imaging (MRI)
Computerized tomography (CT)
Selective laser sintering (SLS)
Stereolithography (SLA)
Digital light processing (DLP)
Mesoporous bioactive glasses (MBGs)
Simulated body fluid (SBF)
Ultraviolet (UV)
Scanning electron microscopy (SEM)
Digital mirror device (DMD)
Fused deposition modeling (FDM)
acrylonitrile butadiene styrene (ABS)
Polylactic acid (PLA)
Polyethylene terephthalate (PET)
Polyvinyl alcohol (PVA)
Polycaprolactone (PCL)
Phosphate-buffered saline (PBS)
Sodium alginate (SA)
Methacrylate collagen (CMA)
Freeform reversible embedding of suspended hydrogels (FRESH)
Alizarin red staining (ARS)
Polyethylene glycol (PEG)
Silk fibroin (SF)
Osteocalcin (OCN)
Poly(glycerol sebacate) (PGS)
Alkaline phosphatase (ALP)
Human umbilical vein endothelial cells (HUVECs)
Hyaluronic acid (HA)
Gelatin methacryloyl (GelMA)
Polyethylene oxide (PEO)
Wood-based cellulose nanofibrils (WNF)
Alginate/gelatin (Alg/Gel)
Adipose-derived stem cells (ASCs)
Alginate-methylcellulose (algMC)
Alginate dialdehyde (ADA)
Mesenchymal stem cells (MSCs)
Extracellular matrix (ECM)

printing resolution against printing scalability/speed trade-off among different types of materials, including biopolymers, metals, glasses, glass-ceramics, and composite materials [8,9]. This allows addressing the limitations of conventional methods and precisely controlling the fabrication process by producing customized scaffolds in a layer-by-layer manner and based on a computer model [10,11]. The Additive Manufacturing of biopolymer-based scaffolds for TE has been confirmed by utilizing several techniques [12,13]. The ideal biomaterial should possess specific biological properties, including biodegradability, biocompatibility, and surface properties (such as cell adhesion) [14,15]. On the other hand, proper integration of scaffolds into the host tissues is of utmost importance for successful implantation. Among various biocompatible materials, bioactive glasses (BGs) have attracted significant attention in tissue engineering owing to their inherent properties (bioactivity, biocompatibility, as well as osteogenic, angiogenic, and exogenous antibacterial activities) [16–18]. They can easily react with body fluids (e.g., plasma) and form hydroxyapatite, which is a natural component of bone, leading to implant bonding to both hard and soft tissues. BGs were shown to enhance osteogenic and angiogenic biomarkers for bone formation via the release of different ions (e.g., silicon and calcium) into the surrounding biological environments [19–21]. Polymer–BGs scaffolds have been researched due to the great bioactivity effects of BGs, which release ions in different types of TE applications. Previously presented papers that evaluated simply anatomically designed BGs-printing scaffolds with certain pore size gradients that mimicked the architecture of several tissues, aimed to improve the overall mechanical behavior and thereby make them suitable for TE [22–24]. Also, recently, a cell-laden approach containing a 3D biopolymer-glass composite can direct cell growth, proliferation, and differentiation [25]. Thus, BG-derived 3D scaffolds are considered an ideal porous template with suitable mechanical properties for use in TE strategies and regenerative medicine.

Herein, we reviewed the application of BGs for the fabrication of 3D-printed and bioprinted (i.e., where cells are deposited along with biomaterials) scaffolds and their usability in TE. For this aim, we explain various fabrication methods utilized for developing BG-based 3D scaffolds with a focus on the additive manufacturing technique. Also, the *in vitro* and *in vivo* studies in which BGs, either alone or in combination with biocompatible polymers, were used as the ink of 3D printed scaffolds are discussed.

2. General 3D printing of BG powder

As mentioned earlier, BGs are effectively used for tissue engineering because of their excellent biological activities. Generally, there are three groups of BGs, including silicate-based, borate-based, and phosphate-based glass. In recent years, many researchers have focused on developing new compositions of BGs to enhance their capacity for osteogenesis, angiogenesis, and antibacterial properties [26–29]. The addition of therapeutic ions into BG networks has been considered to obtain more potent therapeutic materials. Most common dopants include copper (Cu), cobalt (Co), magnesium (Mg), silver (Ag), zinc (Zn), and strontium (Sr) [30]. However, BG applications in the repair of load-bearing bone defects are still limited, especially in porous form, due to their innate high brittleness and low fracture toughness [31]. Moreover, controlling pore interconnectivity, size and overall porosity of BG scaffolds are challenging with utilizing conventional fabrication methods. One solution is employing computer-aided manufacturing (CAM) technologies [32] for making 3D printed BG-based scaffolds with average elastic modulus and compressive strength comparable to human cortical bone. These scaffolds have held hopes for their use in load-bearing applications [33]. Employing controlled architectures using computer-assisted design (CAD) from magnetic resonance imaging (MRI) or computerized tomography (CT) 3D data files of patients as input for 3D printing methods are now able to solve the flaws of the conventional scaffolds and allow the production of customized 3D scaffolds. Direct 3D printing, selective laser sintering (SLS), stereolithography (SLA), digital light processing (DLP), and robocasting are some of these methods [34,35].

Direct 3D printing is stated as a useful approach for producing scaffolds with exact size and porosity. This method attracts much attention for manufacturing strong BG-based scaffolds with porosity around 50 vol% or higher, which is usually employed in bone tissue engineering. The direct 3D-printing method of BG powder begins with a

liquid binder printing on a powder bed, layer by layer, leading to attaching powders along in a preferred range. Following the printing of each layer, another layer is added to the structure by employing a counter-rotating roller. This process will recur until the intended part is printed. Throughout the process, unglued powders act as a support; therefore, complex parts can be identified by pores or undercuts. Removing un-attached powders should be taken into thought in designing the process [36]. During the scaffold sintering, crystalline phase(s) could be developed. Different kinds of bioactive glasses such as 13–93 glass, 45S5 Bioglass®, and mesoporous bioactive glasses (MBGs) are the most common bioactive materials used for producing scaffolds that are employed for the direct 3D printing method. To achieve high-quality scaffolds, there are various parameters to consider. Powders must have good flowability and packing capability since they flow from the feed bed to the printing bed. These important features are precisely adjusted in terms of shape, size, size distribution, and roughness. Spherical particles are mostly better than asymmetric particles for packing. Greater dimensions will result in better flowability; however, it will reduce the resolution. The powder dimension may impact the layer thickness; higher thickness will need more binder while lower thickness leads to a bad resolution as a result of binder flow. Therefore, sizes between 20 and 40 μm are more suitable for avoiding void formation since larger and smaller particles result in the void formation and decreased resolution, respectively. While the porosity of scaffolds made by these materials is typically low (<50 vol%), they are proved to be compatible with load-bearing intents [36,37]. To investigate the effect of porosity (random vs designed) in tricalcium phosphate (TCP)-45S5 Bioglass® porous composites on *in vitro* biocompatibility and compressive strength, Bose et al. [38] produced TCP-BG (45S5 BG) scaffolds using binder jetting-based 3D printing technique (Fig. 1.a). They theorized that adding BG to TCP may control the dissolution kinetics *in vitro* as well as enhance compaction via liquid phase sintering and improve mechanical properties. After adding 5 wt% BG in TCP composites, the compressive strength values were 26.7 ± 2.7 MPa and 21.3 ± 2.9 MPa for the random and designed porosity. In addition, the total porosity was ~ 47.9 % and ~ 54.1 % for random and designed porosity, respectively (Fig. 1.b). Furthermore, interaction with bone cells and dissolution kinetics of the scaffolds were tested *in vitro*. Based on results, TCP-BG compositions exhibited more promising materials for interaction with bone cells as compared to TCP used alone. Also, adding BG boosted a flaky hydroxycarbonate apatite (HCA) layer after 8 weeks *in vitro* (Fig. 1.c). This research also confirmed that fabricating TCP-BG scaffolds using the binder jetting method results in scaffolds with improved properties for bone graft applications [38].

Another method for creating 3D scaffolds is selective laser sintering (SLS), which is performed in one step. In this method, CO_2 or *Nd : YAG* laser scan over the powder bed. The 3D printer comprises a scanning system, a laser, and two different chambers. One of the chambers contains the powder feedstock, and materials are transferred to the other chamber via a roller, building the powder bed layer by layer. When layers are prepared, the laser starts scanning the surface and consolidates the powder. This process will continue until the structure is complete [36]. There are three different binding methods, including solid, liquid-state sintering, and full melting of the particles. Materials

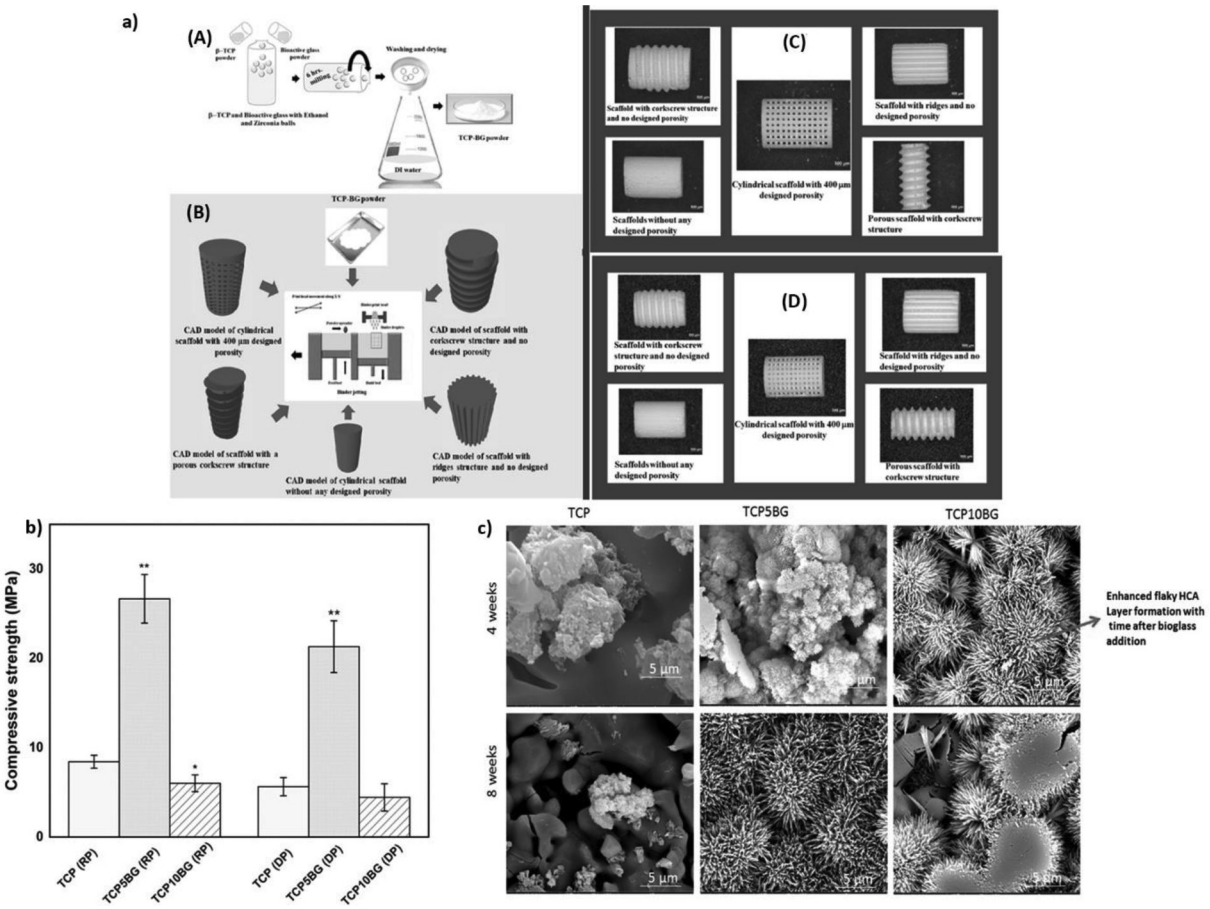

Fig. 1. (a) (Part A) β–TCP and Bioactive glass powders are used in TCP-BG powders synthesis as precursors (Part B) Fabricating TCP-BG scaffolds employing binder jetting method, using 5 different designs as CAD models. (Part C) Different designs of 3D printed green scaffolds using the binder-jet method and (Part D) Sintered scaffolds (2 h at 1250 °C). (b) Morphological image of samples after immersing in SBF for 4 and 8 weeks. As compared to former time points, more intense hydroxycarbonate apatite layers are formed, which increases significantly while adding BG. (c) Compressive strength of designed and randomly porous scaffolds. Copyright Elsevier with permission [38]. (For interpretation of the references to color in this figure legend, the reader is referred to the web version of this article.)

must absorb lights in the laser wavelength range to ensure the process of SLS and the correct formation of the powder bed. In addition, the powder must be flowable. For instance, adding modifiers like Fe_2O_3 in the BG formulation not only darkens the color to absorb the energy of the laser but also increases the efficiency of sintering and lowers the melting point [39]. Compared to the conventional molding process that has a sintering step, the cooling and melting steps in SLS are relatively faster, thus leading to a reduced production time [40]. Liu *et al.* [41] employed the SLS technique to synthesize 45S5 Bioglass®-based scaffolds and adjusted the laser power to achieve the best sintering and densification. According to their findings, higher laser energy (about 20–30 W) could melt the material and give it the ability to flow through layers below. Therefore, higher powers will cause holes and voids in the glass layer [41]. The optimal value of mechanical properties will be achieved when the glass is fully sintered and the residual voids (flaws) inside the filaments are minimized. Even though the heating process was very short, it has been reported that 45S5 Bioglass® undergoes partial devitrification to $Na_2Ca_2Si_3O_9$ during the SLS fabrication [41] which, however, does not suppress bioactivity. For bone repair and regeneration applications, Gao *et al.* [42] reinforced nano-58S BG with different ratios of graphene (0.1–1.5 wt%) to synthesize a scaffold with enhanced mechanical properties using SLS in a *nitrogen* atmosphere for preventing oxidation. Their analyses showed that scaffolds impregnated with 0.5 wt % graphenes improved the compressive strength and fracture toughness up to 105 % and 38 %, respectively. Promising bioactivity and biocompatibility of the composite scaffolds were proved in simulated body fluid (SBF) and cell culture tests. These results suggested that graphene/nano-58S composite scaffolds have great potential for bone tissue engineering applications [42].

In order to reduce required laser power and increase precision, indirect SLS has been employed to produce glass–ceramic scaffolds and pure glass scaffolds. In this process, a post-processing step is introduced, where a binder (which is typically a polymer) is combined with the feedstock and mixed with the powder. After the combination, the binder is melted by laser and holds the glass particles together. The relation between scaffold pore geometry, mechanical properties, and bone regeneration amounts after implantation was examined by Kolan *et al.* [43]. Using indirect SLS, they synthesized borate-based BG scaffolds with five different porosities and five different architectures (cubic, spherical, crossed, gyroid, and diamond) (Fig. 2.a). The compressive strength of the scaffolds varied from 1.7 to 15.5 MPa for 60 % to 30 % porosity, respectively. To examine their bone regeneration potential, cubic and diamond structures were implanted in a rat calvarial defect. Based on the histological analysis, more fibrous connective tissue and mineralized tissue were found in the scaffolds with diamond structure and 50 % porosities, which leads to more potential for faster bone formation (Fig. 2.b) [43].

Stereolithography (SLA) is the most precise method of 3D printing for producing complex structures and gives control over internal architecture with precision down to micrometers, leading to a high-quality surface. In this technique, a photosensitive liquid resin will selectively solidify using an ultraviolet (UV) laser layer by layer to shape a 3D structure. After irradiation of the aforementioned layer, based on the build of the machine (which can be down-top or top-down), the resin bed will be transferred upward or downward as much as the thickness of a layer. When the solid layer is covered by resin, UV exposure will harden it. These steps will iterate until the final structure is achieved [44]. Polymerization happens only in the organic monomer phase since BG particles are inert to UV laser. The viscosity and curing behavior of the filled resins are significantly influenced by the type and volume fraction of the filler and the distribution of particle sizes [45]. The curing depth may be reduced more or less significantly based on the particle size and the index of refraction of the ceramic and photoreactive polymer [46]. This can reduce the resolution of the printed structure and increase the overcuring effect and printing process imprecision [47]. According to earlier research, materials with micro-sized particles can only incorporate up to 40 % of ceramic filler [48]. Uneven distribution of the filler particles inside the printed structure results from poor dispersion and sedimentation challenges. The manufacture of SiO_2, Al_2O_3, and their ceramic derivatives is the main focus of most of the current ceramic SLA research. Very few publications have been published on the SLA fabrication of 3D-printed BGs [49,50]. However, none

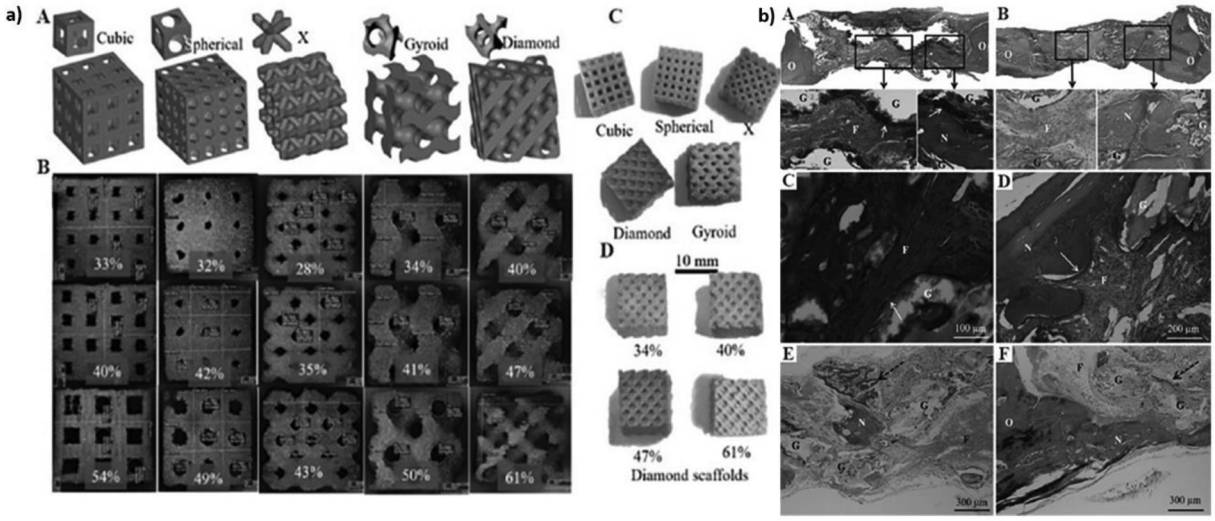

Fig. 2. (a) (A) different scaffold structure and unit cells, (B) optical images of 5 × 5 × 5 mm^3 borate-based BG scaffolds at three different porosities with corresponding architectures (used for compression tests), (C) Each architecture's scaffold with the size of 10 × 10 × 10 mm^3 (measuring porosity), and (D) diamond architecture scaffolds with a size of 10 × 10 × 10 mm^3 at four different porosities (34 % – 61 %). (b) Histological sections defect regions treated after 6 weeks. Hematoxylin and Eosin (H&E) stained sections of (A) diamond scaffold, and (B) cubic scaffold. inset figures show fibrous tissue in pores and arrows show osteoblast cells lining the edges of the diamond glass scaffold strut, (C and D) magnified images of different regions of the diamond scaffold which show newly formed bone tissue, fibrous connective tissue, and remaining glass (E) Masson's trichrome stain showing the glass filament illustrated by arrows surrounded by a pocket of mineralized bone tissue in the pore and the new bone tissue (red), (F) Trichrome stain from the bottom side of the defect, showing that next to host bone, mineralized bone tissue has formed (above dura matter). F – fibrous connective tissue, G – remaining glass, O – original host bone, N – new mineralized bone [43]. (For interpretation of the references to color in this figure legend, the reader is referred to the web version of this article.)

of them have covered the comprehensive examination of the components' effects on the resin's characteristics and photo-curing. Most previous research was essentially focused on evaluating how fabrication and debinding parameters affected the properties of the final BG components [51]. The debinding stage, which is the thermal process aimed to remove organic components, is followed by fusing particles using sintering at high temperatures. One of the key parameters in this method is the type of binder. For example, 3D structures of 45S5-Bioglass® were produced using the SLA method by employing five different types of binders, based on different photocurable and acrylate resins ratios (A (3:7), B (4:6), C (5:5), D (6:4), E (7:3)). Moreover, different volume fractions of this kind of glass (from 32 to 40 % in five different groups) were evaluated in terms of microstructure and optical/physical properties of the suspensions. The (4:6) ratio resulted in the best cure depth, where the volume fraction of BGs has an inverse relation with the cure depth. The flexural strength was reported to vary from 14.0 ± 2.9 to 37.9 ± 5.0 MPa for increasing amounts of 45S5 BG from 32 to 40 vol% in the suspensions. Overall, this study supported the use of 45S5 BG-based suspensions for producing scaffolds for bone regeneration and tissue engineering applications [52]. To better understand how BGs affect the physical characteristics of the resin and the final green body, Chen *et al.* [51] have developed a variety of photo-curable resin formulations with and without BG fillers. In this study, the influence of monomer content, light absorber (dye), a reactive diluent, photoinitiator (PI), and BG percentage on the rheology and photo-curing behavior of the resin and properties of the final 3D scaffolds have been examined. The rheology of the resin was influenced by the BG percentage, which also has an impact on the rate of the polymerization reaction. The resin mixtures containing between 55 % and 60 % BG, 1 % PI, 10 % diluent, and 0.015 % dye were discovered to be appropriate mixtures for the SLA process. The cure depth of the resin was decreased by a higher dye concentration, but over-curing was caused by a higher PI concentration. The finished green bodies were imaged using micro-CT and scanning electron microscopy (SEM), which displayed a rather dense glass scaffold without any observable cracks, strong interlayer connectivity, and a smooth surface. These parameters had a significant impact on the mechanical behavior of 3D scaffolds. This study aided in the development of high density glass and ceramic slurries and enhanced their printing properties [51].

Due to its great accuracy and smooth surfaces, Digital Light Processing (DLP) is one of the most attractive 3D printing techniques [53]. Glass-ceramics [54], calcium/phosphate ceramics [55], and BGs [56] have all been researched as scaffold materials to build patient-based designed structures. The two most common techniques, DLP and SLA, for producing bioceramic-resin 3D structures use visible light with a wavelength of 405 nm and UV light with a wavelength of between 365 and 385 nm, respectively [57]. A digital mirror device (DMD) is used in DLP systems to brighten and recreate each layer simultaneously, often with visible blue light, eliminating the need for a beam to scan the surface. A 2D array of pixels may be recreated by turning on and off the millions of mirrors that comprise the DMD. In this manner, the only time required to form a layer is the one associated with the materials' exposure [40]. Additionally, this technique supports inks with a high solid load of BG/ceramic particles (40 %–60 %) and has an excellent lateral resolution of approximately 40 μm [56]. The DLP technology can be divided into bottom-up DLP and top-down DLP methods according to the position of the light source with respect to the vat containing the slurry. The DLP method can be divided into top-down and bottom-up DLP approaches depending on where the light source is positioned in reference to the tank holding the slurry. The light source can either be positioned above the slurry in a top-down approach or beneath the tank in a bottom-up approach [58]. The use of DLP in the creation of porous ceramic scaffolds with advanced functionality is limited by the high solid content of ceramic slurry. To produce a ceramic-resin slurry with high solid loading, one feasible option is the top-down DLP method [58]. Recently, porous 58S BG/β-tricalcium phosphate (β-TCP-BG) scaffolds with high solid loading were created using the top-down DLP method. To study the effects of solid loading on viscosity and curing reactivity, β-TCP-BG/photosensitive-resin slurries with a range of solid loadings were created. Next, the composite scaffolds' porosity, mechanical properties, microstructure, and shrinkage were investigated. According to the findings, the greatest viscosity of the β-TCP-BG/resin slurry to be printable using this approach was 85.92 Pa s, which was made with 60 % solid loading. As the solid loading increased, the cure depth and overgrowth began to diminish. When the shaping error and sintering shrinkage of the porous structure were evaluated, it was discovered that the minimal pore size and sintering shrinkage values were reached for scaffolds made from slurry at 60 wt%. With increasing solid loading, the compressive strength of the-TCP/BG scaffolds increased, peaking at 11.43 ± 0.4 MPa for solid loading of 60 wt%. In light of this research, the top-down DLP-fabricated β -TCP-BG 3D structure can be identified as a suitable candidate for load-bearing bone tissue engineering. [59].

Robocasting is another method used for fabricating porous 3D scaffolds [60]. In this method, a paste-like ink, formed by combining powder and water with a small number of processing additives (e.g., binders, coagulants, thickening agents, and dispersants) is extruded through a nozzle onto a building platform. In addition to providing mechanical support to the next layers, the used ink should become thinner under shear for facilitating shape retention [31,61,62]. In this regard, a highly challenging process in robocasting is setting the suitable viscoelastic behavior of pastes. Solid loading, particle size distribution [63–65], interfacial solid/liquid interactions [66], and particle shape and density [67] are the most relevant and decisive parameters for the rheological behavior of the starting suspensions.

For bone applications even in load-bearing areas, robocasting is proved to be a very valuable technique in the production of BG scaffolds. This method allows fabricating glass structures with total porosity between 50 and 70 vol% and pore dimensions in the range of a few hundreds of micrometers to more than half a millimeter, due to the ability of this technique in using particles with 1–30 μm of size and extrusion nozzles with diameters in the range of 100–580 μm [40]. Liu *et al.* used 13–93 glass to produce robocast grid-like scaffolds with porosity of 47 vol% and pores with a size of 300 μm, and investigated their mechanical properties *in vitro* after immersion in SBF solution and using a rat subcutaneous model *in vivo*. Scaffolds implanted *in vivo* showed a change from brittle to elastoplastic mechanical behavior, presenting a bone-like response; furthermore, the mechanical properties exhibited a reduction after 2 weeks *in vitro* and *in vivo*, while remaining high enough for potential load-bearing application [68]. Using a carboxymethyl cellulose-based ink, Eqtesadi *et al.* [61] synthesized robocast vitreous scaffolds that showed porosity between 60 and 80 vol% and compressive strength of 2–13 MPa, which was comparable to the trabecular bone [61]. Barberi *et al.*[69] used the robocasting technique to fabricate completely amorphous scaffolds with a porosity gradient and grid-like structure, resulting in a denser core. Their results were very promising for future bone defect repair applications based on suitable porosity, mechanical strength, and *in vitro* bioactivity [69]. In another research, Dixit *et al.* [70] used functionalized multiwall carbon nanotube (MWCNT-COOH) to enhance the compressive strength and decrease the brittleness of borosilicate bioactive glass (BG-B30) 3D scaffolds synthesized by the robocasting method. Their results showed that the mean compressive strength of pure BG-B30 scaffolds was 23.30 MPa, while MWCNT-COOH reinforcement enhanced the compressive strength up to 35.84 MPa. The high bioactivity and cell viability of these carbon nanotube-reinforced BG porous scaffolds indicated that they could be promising for bone tissue engineering applications [70]. Fig. 3 shows the principles of these five techniques (direct 3D printing, SLS, SLA, DLP, and robocasting). Also, some advantages and disadvantages of these techniques for 3D-printing of BGs powder and polymer/BG composites are summarized in Table 1.

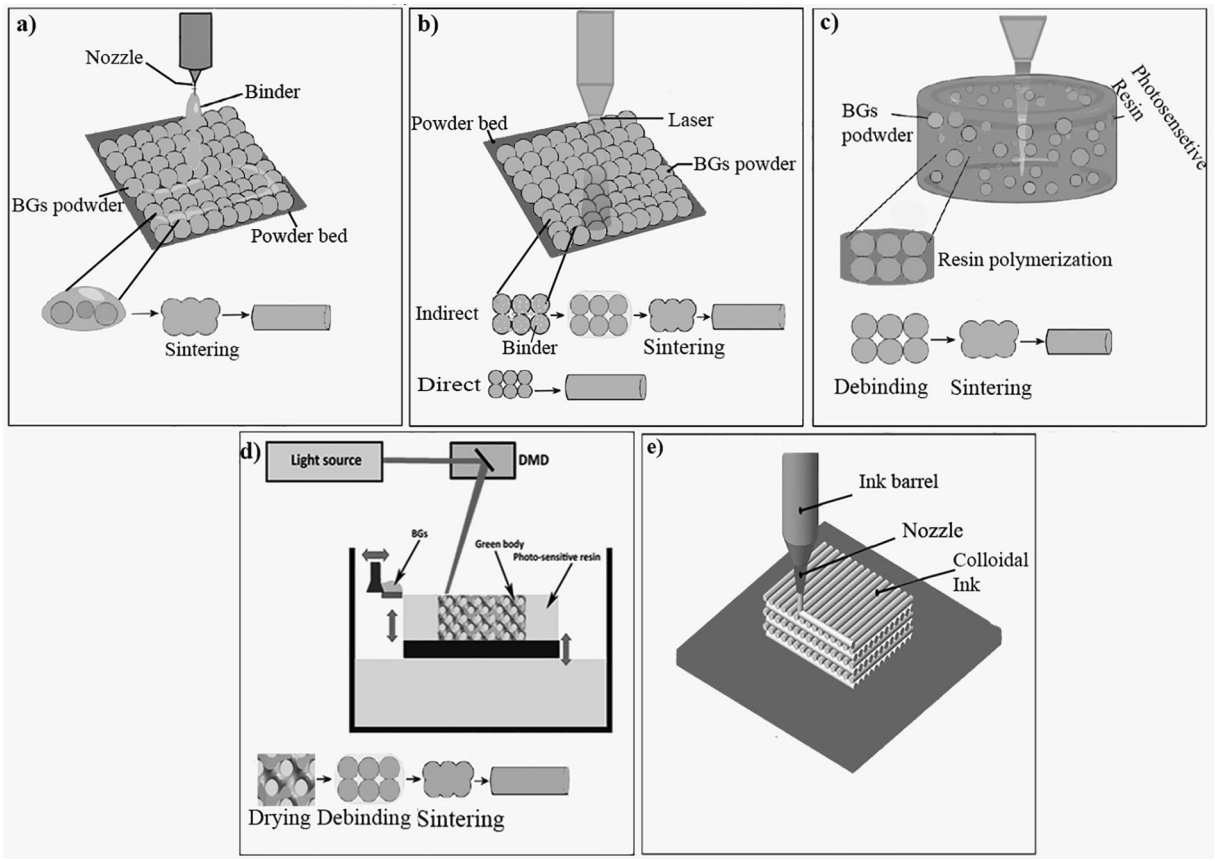

Fig. 3. Schematic of different manufacturing techniques using additives including (a) Direct 3D printing, (b) selective laser sintering (SLS), (c) stereolithography (SLA), (d) digital light processing (DLP), and (e) Robocasting for 3D printing bioactive glasses powder.

3. 3D printing of polymer/BG composites

In order to build an ideal scaffold for mimicking bone tissue structure, the fabrication of composites has provided great opportunities in tissue engineering and regenerative medicine. BGs with inherent osteogenic and angiogenic features are mentioned as substitutes for the inorganic phase of bone. On the other hand, polymeric materials are used as suitable materials for replacing the organic phase of bone tissue. This led to preparing a composite scaffold with improved physicochemical, mechanical, and biological characteristics [78].

Extrusion-based 3D printing is the layer-by-layer deposition of semi-molten or molten polymers, polymer solutions, dispersions, or pastes in a direct ink writing mode via a moveable nozzle acting as the extrusion print head [11,79]. Melting-based processes, such as fused deposition modeling (FDM), melt electrospinning writing, and dissolution-based processes (e.g., 3D plotting) are types of extrusion-based 3D printing [80]. The most widely used extrusion 3D printing technology is FDM. In FDM, a strand of filament or granule is first loaded into a 3D printer. The string is supplied to the extrusion head and into the nozzle of the melted object after the nozzle achieves the desired temperature. The extrusion head is attached to a three-axis system that allows it to move in three directions: X, Y, and Z. The extruder's molten material is injected and cooled in thin strands, layer by layer, in predefined locations. Once a layer or sheet is finished, it moves down and prints the next layer [81–83]. This process continues until the model is completed. Some of the most often used printing materials for FDM are acrylonitrile butadiene styrene (ABS), thermoplastic polyurethane, polylactic acid (PLA), and polyethylene terephthalate (PET). Breakaway materials, polyvinyl alcohol (PVA), and wax are examples of water-dissolvable support materials that are removed during post-processing [84,85]. When the production of polymer-BG composites is a goal, inorganic particles have to be added to the organic matrix before the printing process. Employing an FDM 3D printer, Fathi *et al.* fabricated scaffolds of polycaprolactone (PCL)/BGs for potential use in bone tissue engineering applications. BGs were used to improve the cytocompatibility of the PCL constructs. Incubation of the constructs with MG-63 osteosarcoma cells for 24 h revealed no adverse effects on cell growth and proliferation. Additionally, MG-63 cells were properly attached to the scaffolds and expanded on them. Cells attached better to the scaffold surfaces after BG incorporation into PCL due to increased hydrophilicity, and the mechanical strength of the BG-containing constructs showed a sharp improvement. After 14 days of incubation in SBF, globular agglomerates formed on the surface of the 3D-printed scaffold, creating a hydroxycarbonate apatite-like layer which is key for bone bonding and osteogenesis [86].

Synthetic and natural polymers, functional polymers, polymer compounds, and cell-rich polymeric systems are usually applied for the fabrication of hydrogels. Among them, hydrogels made of collagen, fibrin, gelatin, and alginate represent the most applicable classes of materials used in the 3D printing of bone tissue constructs [80].

Extrusion 3D printing of hydrogels has been examined in recent years. In order to build 3D structures properly in this manner, the first layer must be structurally sound before the second layer is applied [87]. As a result, features such as the gel-forming mechanism and polymer rheology are critical; polymer solutions must first be viscoelastic or viscous, and then self-supporting gels must be generated before adding further layers. Temporal gelation management is crucial to avoid premature gelation of the polymer solution while it is still in the printer; these crucial aspects have been comprehensively reviewed elsewhere [88]. Several printing processes for hydrogel-forming polymers are provided for this purpose [89]. Polymers that generate hydrogels primarily by physical interactions (e.g., gelatin, agarose, collagen, and methylcellulose) have a gel transition temperature below the amounts in

Table 1
Summary of the different types of 3D-printing of BGs powder and polymer/BG composites with key advantages and disadvantages.

3D-printer	Ink	Advantages	Disadvantages	Ref.
Direct 3D printing	BG powder + a liquid binder	-Possible usage of BGs powder with large granules. -Appropriate mechanical properties. -Excellent structural precision in the sub-millimeter range.	- Crystallization of BGs during sintering.	[71,72]
SLS (direct and indirect)	-BGs -BGs + Binder (e.g., stearic acid)	- Capacity for use in non-load-bearing applications. - Fabrication of macroporous structure.	- Weak mechanical properties. Crystallization of BGs during the process.	[73–75]
SLA and DLP	-UV-curable resin (e.g., acrylate/epoxy) + BGs -Photo-sensitive resin (e.g., monomer PEGDA + BGs	- Ability to adjust pore structure. -High fracture resolution.	- High difference in refractive indices between photo-reactive polymers and BGs particles -Limitations in particle size and distribution - Lack of photo-curable polymers accessible	[53]
Robocasting	paste-like ink (BGs + water + processing additives)	- Easily incorporate various biomaterials when printing.- Possible mixing of diverse organic phases (BGs or ceramic) and inorganic phases (polymers, drugs, and bioactive molecules) - Fabrication of porous or dense BGs components for load-bearing purposes	- Low fracture resolution. -Fabrication of extremely delicate and sophisticated structures	[69,76]
FDM	Natural or synthetic polymer + BGs	- Increasing mechanical properties - Uniform printable filament	- Concentration limit - Limitation on particle size and dispersion	[77]

Abbreviations: SLS; Selective laser sintering. SLA; Stereolithography. DPL; Digital light processing. PEGDA; Poly (ethylene glycol) diacrylate. FDM; fused deposition modeling.

which solution gels develop [90]. Hot solutions of these polymers can be printed onto a cooled stage, where they reach their gel transition temperature and solidify [91]. Physical hydrogels are fragile and may require reinforcement with additional polymers or a post-print crosslinking technique, which is stated as a drawback of this method. In terms of temperature drop magnitude a compromise must be made; the polymer solution will have a high viscosity and require high pressure to eject if the temperature drop is small; however, it will take a long time to cool down and gel if the temperature drop is considerable [92]. The initial and end temperatures of the polymer solution/gel transition may also prevent the inclusion of cells during printing in some cases, as temperatures outside of typical body ranges could harm the living material. Photo-curable hydrogels can be printed onto an illuminated stage and produce hard hydrogels upon exposure to light [93]. Some polymers such as collagen, fibrin, and gelatin can be directly photocured if the right photoinitiator is used [94].

Alginate is a natural, negatively charged polysaccharide made from brown algae. Alginate is widely used in bone remodeling due to its biocompatibility, high water absorption capacity, non-immunogenicity, capability to be functionalized with adhesive cell ligands, and low cost [95]. However, alginate has less cell adhesion than other natural polymers. To solve this problem, some researchers combined it with other natural polymers such as fibrinogen and gelatin [95,96]. Because the rate of alginate degradation is slow and unpredictable, it also exhibits poor mechanical strength, bioactivity, and osteoconductivity. Alginate can be combined with bioactive materials to improve its properties [97,98]. BGs can be combined with alginate to improve their biological performance in terms of reactivity [99]. Wu *et al.* applied the extrusion 3D printing for developing a sustained release hydrogel scaffold consisting of sodium alginate, gelatin, and MBG for potential use in the regeneration of bone defects. They used naringin and calcitonin gene-related peptides as a drug and also studied the biocompatibility of the scaffold and its effect on bone proliferation and differentiation of MG-63 cells, which are similar to human osteoblasts. Their results showed that these scaffolds were potent osteoconductive materials due to their high porosity. In addition, scaffolds containing BGs have shown excellent biodegradability, biocompatibility, and cell adhesion, and this type of composite hydrogel has good potential in repairing bone defects. The scaffolds were loaded with naringin or calcitonin gene-related peptides using a variety of approaches like surface absorption and including direct printing. The pores were connected along the depositional direction, with pores between the pillars measuring 400–600 μm in diameter, 80 % total porosity, and multi-level microspore structures on the pillar surfaces. The composite hydrogel scaffolds showed a rapid rate of water absorption within the first 10 min after soaking for 8 h, and a steady swelling rate of 3.35. The scaffolds deteriorated by 5 % after immersion in phosphate-buffered saline (PBS) without lysozyme for 35 days [100]. In another study, Luo *et al.* made alginate and 13–93 BG scaffolds using extrusion-based 3D printing under mild conditions with an XXYY pattern. As shown in Fig. 4, printable inks were then prepared by mixing sodium alginate (SA) powders and 13–93 BG powders with PVA. A printing needle with a 406 μm diameter and a computer-assisted design was used to produce the scaffolds (Fig. 4. A (a)). The composite inks were extruded at a constant dispensing speed of 25 mm s^{-1} with dosing pressures varying from 400 to 500 kPa. To do crosslinking, the prepared scaffolds (Fig. 4. A (b)) were soaked in $CaCl_2$ aqueous solution and then lyophilized for use in subsequent experiments (Fig. 4. A (c)). Their results showed that the addition of BG improved the mechanical properties and increased the apatite mineralization. In addition, alginate/BG composite scaffolds provided a good substrate for cell adhesion, and mesenchymal cells were able to well differentiate into bone cells (Fig. 4. B) [101].

Gelatin is a fibrous protein that is obtained by denaturing the collagen triple helix structure into single-stranded molecules [102]. Gelatin has good biocompatibility, high water absorption, non-immunogenic, and biodegradability. Gelatin is heat sensitive and

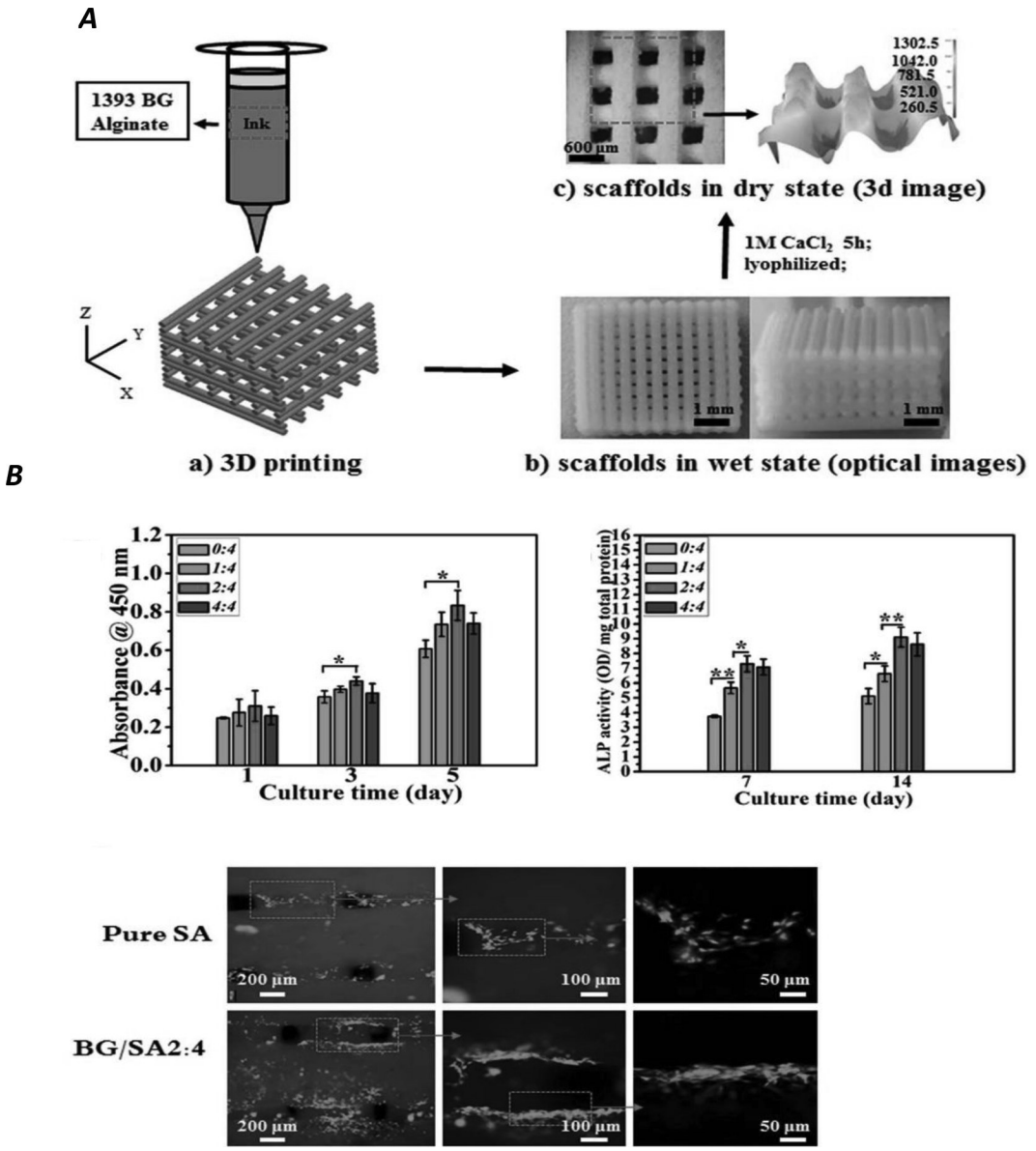

Fig. 4. (A) Fabrication process for 13–93 bioactive glass/sodium alginate composite scaffolds: (a) A computer-aided design model and bio-inks; (b) optical pictures of wet scaffolds; and (c) a 3D image of dried scaffolds. (B) Response of rBMSCs to BG/SA composite scaffolds produced in 3D printer [83].

becomes a viscous liquid at 37 °C and can be easily printed using extrusion-based printing, while at lower temperatures it forms a gel by hydrogen bonding [103].

In this regard, Bertuola et al. investigated the rheological properties and printability of gelatin-alginate-hyaluronic acid inks incorporating different concentrations of 45S5 BG particles (2 to 8 %wt) by using extrusion-based printing and with Ionic interaction crosslinking method. The addition of BG reduced the storage modulus as well as the viscosity of the inks and disrupted the polymer network, and the modulus of the tensile strength of the scaffolds was increased along with increasing the BG percentage. In addition, inks without BG or with a low percentage of BG (2 %) showed the best printing fidelity, while printing fidelity decreased with increasing BG concentration. On the other hand, a layer of hydroxyapatite formed on scaffolds containing a high percentage of BG after 2 days of culture, indicating the potential of these scaffolds in bone tissue engineering applications. This type of scaffold could also provide good biocompatibility and cell adhesion [104].

Collagen is a biocompatible protein with suitable physical properties, a triple helix protein with cell-binding sequences in its structure that can help cells to attach, proliferate and differentiate [105]. It is now clear that the bone ECM consists of the deposition of apatite minerals in the type 1 collagen substrate; therefore, collagen is an excellent candidate for the 3D printing of bone tissue [106]. To simulate bone regeneration, Kajave *et al.* made ink containing methacrylate collagen (CMA) and Bioglass 45S5 using 3D printing techniques and photochemical crosslinking. The presence of BG particles in the collagen scaffold increased the stability and reduced the swelling of collagen hydrogels. After the inclusion of BGs, rheological testing revealed a considerable improvement in the yield stress and recovery percentage of 3D-printed structures as well as better bone bioactivity and cell viability. In addition, cell-mediated calcium deposition in the CMA/Bioglass® 45S5 ink-based structures was significantly higher compared to the CMA alone, which confirmed good potential in bone tissue engineering. To create stable 3D constructions, the CMA and the BG-CMA inks were printed in a freeform reversible embedding of suspended hydrogels (FRESH) support solution and cross-linked with UV. Alizarin red staining (ARS) was very faint in the CMA composites without BG. BG-CMA constructs, on the other hand, were heavily stained with ARS, indicating that BG was

present within the printed BG-CMA constructs and enhanced osteogenesis [107]. Schuhladen *et al.* made a composite ink based on methylcellulose, manuka honey hydrogels, and borate BG and extruded it using a 3D printing technique with physical crosslinks, based on the ion-release effect from glass particles (Fig. 5. A-B). Their results showed that the printing ability of the inks was improved with the addition of BG and the scaffold showed good swelling behavior and mechanical properties [108].

The molecular structures of polymers largely dictate their capabilities for 3D printing. Widely used polymers in 3D printing of bone-mimicking constructs include PCL, polyethylene glycol (PEG), and PLA.

Using the FDM technique (Fig. 6. A), Distler *et al.* created PLA/BG composite scaffolds for possible use in bone tissue engineering. This research group evaluated the printing capability of PLA/BG filament and the biocompatibility and bioactivity of the scaffold by using MC3T3E1 cells. In addition, the printability of BG was investigated (Fig. 6. B). Open-porosity scaffolds with a height of 12 mm and a diameter of 10 mm were created (Fig. 6.C) [109]. The results revealed that the presence of BG powders increases the osteogenic differentiation of adipose-derived human stem cells *in vitro*.

PCL is extensively utilized in extrusion printing due to its high stability, low melting point, as well as good rheological and viscoelastic properties [110]. Melt-extrusion modeling is one of the most common 3D printing methods. This technique uses a plastic material that is fed into an extrusion nozzle. The extrusion nozzle is heated to melt the plastic material. The molten material is then poured into very small beads in one step. The plastic is removed from the heated nozzle, cooled quickly and hardened, and bonded to the layer on which it is placed. Before starting the printer for the next layer, one layer is completed and thereby a layer-by-layer model is gradually created [111]. Kim *et al.* created a PCL composite scaffold containing $CaO\text{-}SiO_2\text{-}P_2O_5\text{-}B_2O_3$ bioactive glass (BGS-7) by using a melt-extrusion process. The toughness of composite scaffolds was greatly improved compared to the pure glass scaffolds with similar porosity [112]. Using MC3T3-E1 cells, the biological properties of the scaffolds were investigated, and the results revealed that the cell proliferation and osteogenic activity were significantly increased along with an increase in the glass weight percentage. In addition, PLA polymers are also mainly used in laser printing techniques. PLA is a biodegradable, biocompatible, non-toxic, polyester-based polymer and is considered in bone tissue engineering because of its excellent properties [113,114]. Using the extrusion 3D printing, Estrada *et al.* created a scaffold containing 45S5 BG and PLA provided with macro- and microarchitectures. They synthesized BGs by the sol–gel process assisted with microwave exposure. Upon immersion in SBF, a layer of hydroxycarbonate apatite formed on the surface of the scaffold owing to the presence of bioactive glass inclusions, and the composition and printing parameters were properly optimized to obtain a suitable scaffold design as well as chemical and mechanical properties for use in bone regeneration [115].

MBGs are known as promising platforms for the loading and delivery of drugs. They are also ideal materials for use in bone tissue engineering [116]. The combination of MBGs and a polymer can enhance both the biological activity of the pure polymer and avoid the drawbacks of the inorganic material used alone, such as high fragility [117,118]. To use the beneficial properties of silk fibroin (SF) and MBG simultaneously, Du *et al.* printed SF/MBG composite scaffolds and compared them with PCL/MBG as a control group (Fig. 7.a) [119]. The compressive strength of SF/MBG scaffolds was notably higher than the PCL/MBG group therefore SF can be an ideal material for bone repair (Fig. 7.b). SEM images and EDS spectra of two sample groups after soaking in SBF for 5 days showed the stability of these constructs and also an apatite layer formed on the surfaces of both groups (Fig. 7.c). The interaction between cells and biomaterials is crucial in cell attachment and proliferation. *In vitro* cell viability assay revealed that both 3D-printed scaffolds were biocompatible because cells well adhered to the surface of scaffolds. In comparison to the PCL/MBG scaffolds, hBMSCs expanded better on the surface of SF/MBG structures due to their smooth flat struts (Fig. 7.d). H&E staining of subcutaneously implanted hBMSCs-loaded SF/MBG and PCL/MBG structures into the back of nude mice demonstrated that hBMSCs grew appropriately on both scaffolds (Fig. 7.e). Osteocalcin (OCN) staining for testing the osteogenic differentiation ability of scaffolds showed that SF/MBG structures had a higher differentiation ability than the control group (Fig. 7.f). Generally speaking, MBG/SF scaffolds revealed promising properties for use in bone tissue engineering [119].

As mentioned above, MBGs are employed in bone regeneration strategies due to their bioactivity, regular mesoporous structure, and ability to load and release drugs. To evaluate the delivery of the anti-tuberculosis drug, Pei *et al.* constructed an MBG/metal–organic framework (MBG/MOF) scaffold using the 3D plotting method. Their results showed that the fabricated scaffolds consisted of a network of pillars layered on top of each other, resulting in uniformly large cavities, and had high compressive strength. Also, MBG/MOF scaffolds showed the ability to form apatite and good biocompatibility due to the presence of MBGs. In addition, the drug release rate could be controlled and had no effect on biocompatibility or bioactivity owing to MOF degradation. Overall, these scaffolds exhibited high potential for the treatment of osteoarticular tuberculosis with the delivery of a stable anti-tuberculosis drug [120].

3D printing can be combined with electrospinning to create multi-layer polymer/glass scaffolds with multi-scale porosity. These compounds are mechanically resistant, biodegradable, and biocompatible with the ability to release bioactive components. In an experimental study, Touré *et al.* directly electrospun PCL and poly(glycerol sebacate) (PGS) fibers on one side of 3D-printed grids of PCL-PGS blends

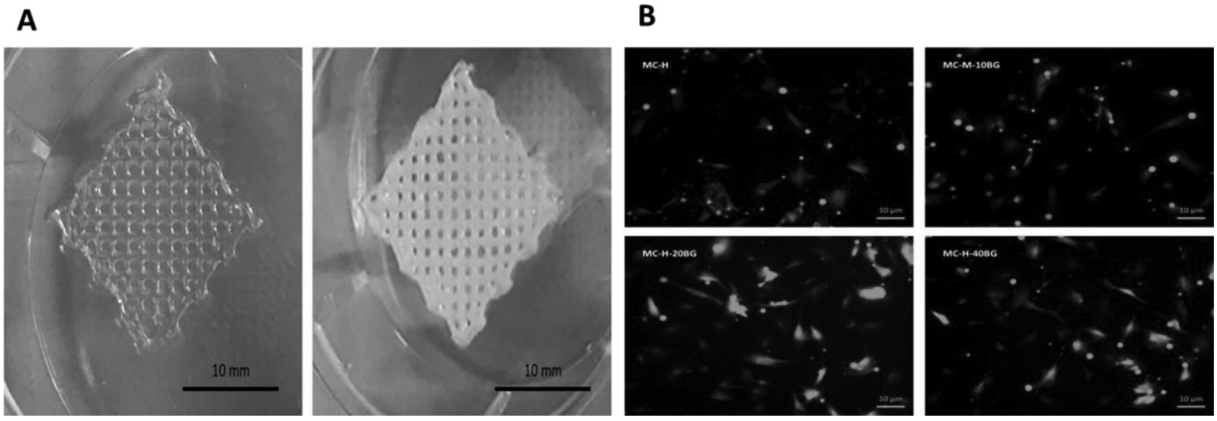

Fig. 5. (A) 3D-printed methylcellulose–manuka honey hydrogel with incorporated borate BG particles. (B) 24 h after cell seeding, fluorescent pictures of human dermal fibroblasts (hDFs) grew on Methylcellulose–manuka honey scaffolds containing various concentrations of borate BG particles [108].

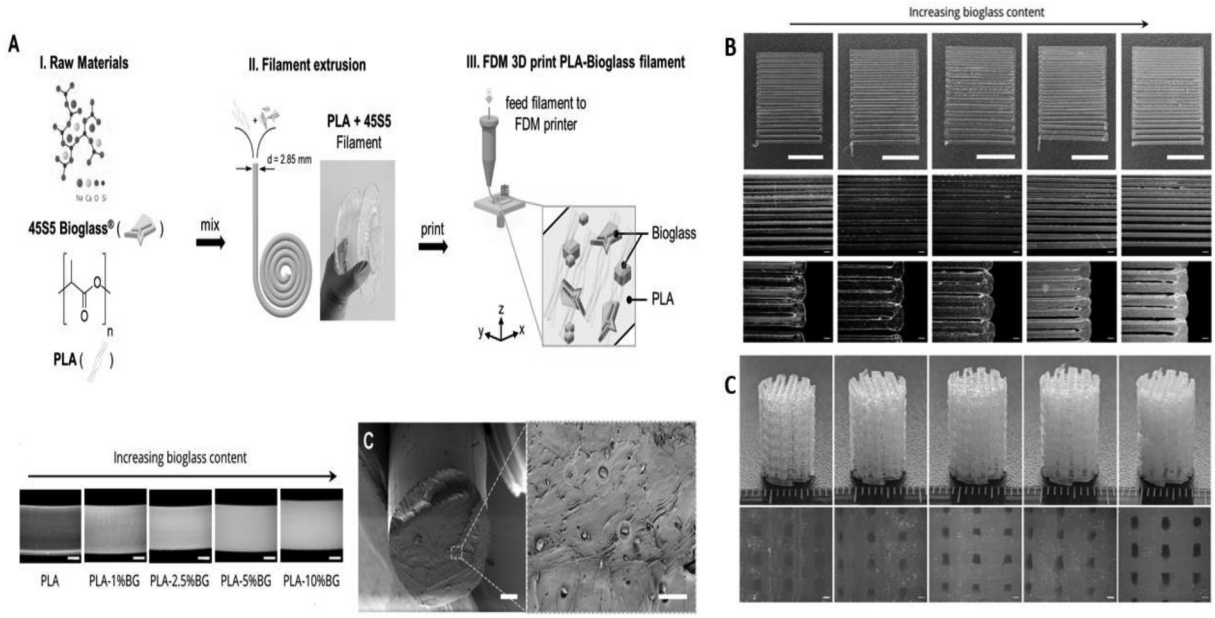

Fig. 6. (A) PLA-45S5 BG filaments fused deposition modeling. (B) PLA-BG filaments are tested for printability. (C) PLA-BG scaffolds 3D printed with FDM from pre-made filaments.PLA-0 % (wt) BG, PLA-1 % (wt) BG, PLA-2.5 % (wt) BG, PLA-5 % (wt) BG, and PLA-10 % (wt) BG 45S5 are shown from left to right [109].

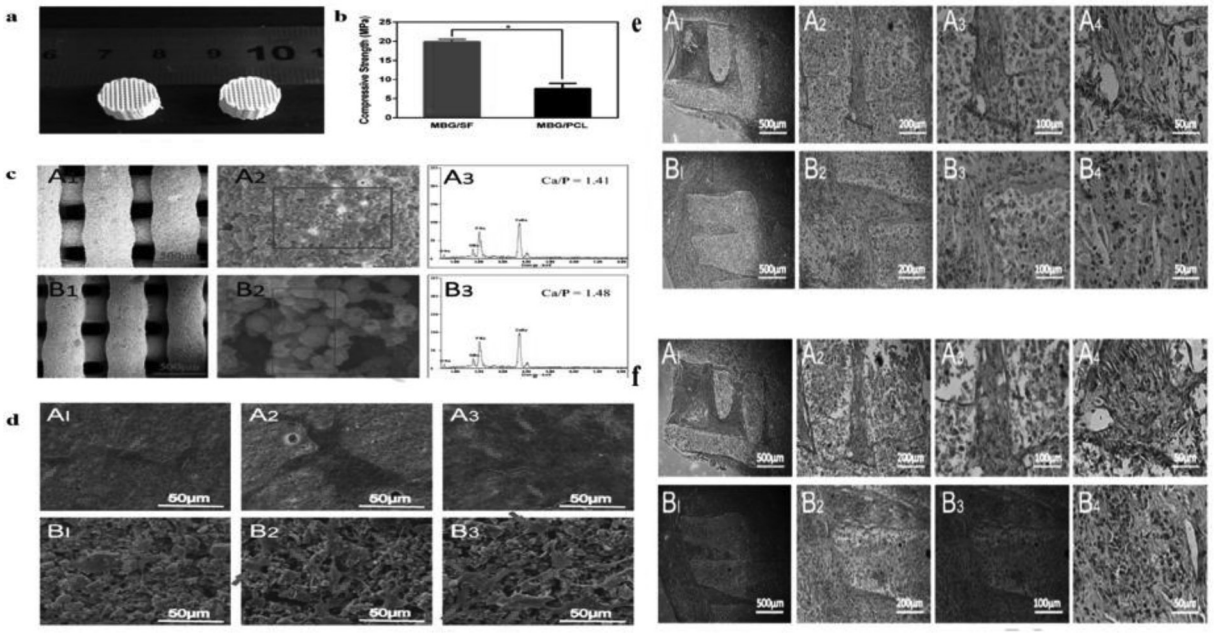

Fig. 7. (a) Optical image of MBG/SF (b)Compressive strength and (c) SEM images of MBG/SF and MBG/PCL scaffolds after soaking in SBF for 5 days (A1 & A2 represent MBG/SF; B1 & B2 represent MBG/PCL) and EDS spectra (A3 represents MBG/SF and B3 represent MBG/PCL scaffold). (d) SEM images of hBMSCs on (A) MBG/SF & (B) MBG/PCL structure for 4 and 7 days. The red arrows show cells. (e) H&E staining and (f) OCN staining of *in vivo* bone heterotopic bone formation assay of MBG/SF (B) MBG/PCL [119]. (For interpretation of the references to color in this figure legend, the reader is referred to the web version of this article.)

containing BGs [121]. This scaffold showed good adhesion among the layers and good degradability. Cytotoxicity experiments showed that PCL-PGS-BG constructs have good compatibility with fibroblasts. The use of this method led to promising results that can make a proof for their use in tissue regeneration approaches.

Scaffolds with suitable biomechanical properties to withstand the load is a critical issue for the treatment of bone defects. BG-polymer scaffolds with ion release may stimulate osteogenesis *in vitro* and *in vivo*. However, scaffold fabrication methods usually require the use of solvents that cause surface changes on BG particles. In this case, the mechanical properties of the scaffold are compromised. Daskalakis *et al.* used a simple melt mixing approach to produce PCL/BG pellets to make scaffolds with controllable pore sizes. Their results showed that the addition of BG particles improves the mechanical properties of the scaffolds and, as a result, all scaffolds provided excellent mechanical properties for use in the cortical bone area. Furthermore, the addition of BGs had shown a long-term effect on the biological performance of scaffolds [122]. Modified MBG scaffolds (MBG-β-TCP) with hierarchical porous structure and suitable functional surfaces were successfully prepared through 3D printing and rotating coating. After applying this

method, the mechanical strength and mineralization of MBG-β-TCP scaffolds were significantly increased in comparison to MBG-free β-TCP scaffolds. Cell adhesion, alkaline phosphatase (ALP) activity, and angiogenesis-related gene expression (VEGF and HIF1-α) of human umbilical vein endothelial cells (HUVECs) in MBG-β-TCP scaffolds showed a significant increase compared to those without MBG. Experimental results show that the use of MBG nanofiber for modifying 3D printed bioceramic scaffolds is a new approach to making hierarchical porous scaffolds with tunable chemical, mechanical and biological properties [123].

4. 3D bioprinting of BGs

Overall, the bioprinting method – in which living cells are incorporated in the printable ink –includes three main phases: (I) the pre-bioprinting phase, (II) the bioprinting phase, and (III) the post-bioprinting phase. In the pre-bioprinting phase, the model of the scaffold for printing is prepared by processing CT scans, MRIs, or CAD models. Besides, in this phase, a solution known as bioink should be prepared [124]. In the pre-bioprinting phase, the selection of cells and materials for making an appropriate bioink for bioprinting is crucial [125]. In the next phase, i.e. bioprinting phase, the bioink is placed into the bioprinter syringe or cartridge and printed. After bioprinting, the structure must be maintained in good condition to guarantee the growth and proliferation of cells through the materials. To provide this condition, the construct should be placed into a bioreactor to mimic the body environment in the post-bioprinting phase [124,126].

Bioinks should be separated from biomaterial inks. Biomaterial inks could be printed by 3D printers and sterilized; cells could be seeded on the scaffolds after printing. On the other hand, bioinks are materials that contain cells and bioactive molecules at the same time [127]. Bioinks affect the phenotype of encapsulated cells and thus activate different cell signaling pathways and the expression of different related genes [128]. Generally, there are two types of bioinks available: scaffold-free and scaffold-based bioinks. By using scaffold-free bioinks. The embryonic process of development imitates the creation of a neotissue. In this method, functional tissues are created on a large scale using tissue spheroids, cell pellets, and tissue strands [129]. Despite being cell-friendly and having rapid tissue maturation and production, these bioinks have several disadvantages such as minimal scalability, a requirement for high beginning cell populations, and insufficient mechanical integrity [130]. On the other hand, in scaffold-based bioinks, cells are put into structures including hydrogels, microcarriers, or decellularized matrix [129]. It is easy to bioprint this type of bioinks. Furthermore, they are scalable, affordable, and high resolution. Nevertheless, there are several limitations to these bioinks, including their toxicity, degradation, and limited ability to interact with cells [130].

Among different bioinks, hydrogels are considered a supreme tissue engineering material because of their unrivaled biochemical and physical properties, high content of water, and biodegradability. Additionally, the capacity of holding water and the softness of hydrogels are similar to the physiological conditions of the human body [131]. Of course, the swelling capacity of bioinks should be minimum and the materials should preserve their shape after printing [132]. Natural or synthetic polymeric hydrogels have all found a variety of uses in bioprinting (alginate, agarose, chitosan, collagen, gelatin, fibrin, HA, GelMA, Matrigel, Pluronics, PEG, etc.). Their nature of being ion-, photo-, thermo-, enzyme-, or pH-sensitive allows them to be gelled easily to create structures in bioprinting process [129]. For hydrogels, having a quick crosslinking mechanism is crucial. Cross-linking process modifies the internal structure of the hydrogel to acquire the desired mechanical properties. Depending on what causes the reaction, crosslinking can be carried out in one of the three main ways: Physical (heating or cooling, hydrogen bonding, ionic interactions, etc) [133], chemical (photo-irradiation, crosslinking agents, etc.) [134], or enzymatic. In the body, crosslinking of ECM proteins has occurred through enzymatic reactions [135].

As mentioned earlier, BGs enhances osteogenesis and angiogenesis and may have inherent (i.e., composition-related) or “exogenous” (after drug incorporation) antibacterial properties [26–29]. Therefore, adding BGs to the bioinks stimulates the stem cells to differentiate into osteoblast cells [136]. This process is one of the most important ways to repair bone tissues [137].

Four different techniques are available for bioprinting [138], including (I) inkjet bioprinting, (II) extrusion bioprinting, (III) stereolithographic bioprinting, and (IV) laser-based bioprinting (Table 2).

Inkjet bioprinting is a non-contact method. This approach suffers from some limitations because of its inability to provide a continuous flow. However, three different types of inkjet bioprinting are available, including (I) continuous-inkjet bioprinting, (II) electro-hydrodynamic jet bioprinting, and (III) drop-on-demand bioprinting [150]. Due to unique advantages like the capability of delivering biomaterials, drop-on-demand bioprinting is more popular [142]. In this technique, droplets of a diluted bioink are printed on a predefined platform by using thermal or acoustic forces. A thermal printer utilizes heat to produce a pressure pulse in a print head and an acoustic one uses piezoelectric crystals to apply a voltage and acoustic wave to change the shape of droplets. These forces cause droplets to be ejected from the bioprinter’s nozzle [151,152]. Material selection is very important in this technique. Potentially suitable materials must be viscous enough to avoid clogging the nozzle while still being rigid enough to endure mechanical forces [153]. Some challenges in this method are listed below:

- The bioink should be dissolved in water and pH, osmolarity, and ion concentration should be adjusted in a way to resemble the physiological conditions.
- Printed cells should not be dried and spread after printing.
- Physical stress on cells while ejecting from the nozzle should be considered [154].

A modified thermal inkjet bioprinter was used by Gao *et al.* to assess the osteogenic capability of bioprinted hMSCs embedded into PEG dimethacrylate containing BGs 45S5 and/or hydroxyapatite. Compared with PEG scaffolds, the mechanical strength of PEG-HA and PEG-BG-HA scaffolds was lower either for cell-laden or without cells structures. Nonetheless, the mechanical strength and stiffness of cell-laden scaffolds showed an enhancement after three weeks in culture, probably because of higher amounts of ECM secreted by cells. Moreover, the PEG-BG group showed the lowest compressive modulus among all groups and the mechanical strength of these scaffolds did not change after 3 weeks. In addition, the constructs with hydroxyapatite revealed the highest level of cell viability and collagen type I, osteocalcin, and MMP13 expression. In summary, this study demonstrated the feasibility of bioprinting bone-like tissue and the positive effect of using BGs in promoting osteogenesis [155].

Another technique for bioprinting is extrusion bioprinting. In this method, polymer or hydrogel strands are dispensed via a micronozzle and located through the computer-controlled motion from the printing head or collection stage. In this approach, bioink is put into metallic or plastic syringes and driven by piston, screw, or pneumatic pressure systems [156,157]. By this technique, the resolution of 200 μm could be achieved which is considerably lower in comparison with inkjet or stereolithography bioprinting. When bioink flows through the nozzle, it is under high pressure. Therefore, the rheological characteristics of bioink, especially shear thinning characteristics, are crucial [158]. Many factors must be considered to design/choose an ideal bioink, including biocompatibility and printability of bioink. The printability of bioink depends on the surface tension and viscosity of the solution [159]. Ojansivu *et al.* evaluated the effect of BG and wood-based cellulose nanofibrils (WNF) on rheological properties and cell response of alginate/gelatin (Alg/Gel) bioinks. They reported that hydrogels containing BGs have higher viscosity and more SaOS-2 cells died immediately after

Table 2
Advantages and limitations of different 3D bioprinting methods.

Bioprinter Model	Bioprinter types	Bioprinter subtypes	Cell density (mL^{-1})	Cell viability (%)	Bioink viscosity (mPa.s)	Resolution (μm)	Advantages	Limitations	Ref.
Inkjet bioprinting	Drop-on-demand bioprinting Electro-hydrodynamic jet bioprinting Continuous-inkjet bioprinting	Piezoelectric Thermal Electrostatic	10^6	90 70–95 >70 90	3–30	37–100	- Nearly high resolution - Speedy fabrication - Inexpensive approach - Various materials	- Low cell density - Force stressor - Nozzle clogging - Inability to reach a continuous flow with low viscosity bioinks	[139–143]
Extrusion bioprinting	Pneumatic extrusion Piston extrusion Screw extrusion		10^8	40–97	30–10^7	200	- High cell density - Ability to use multiple biomaterials with multiple nozzles - Nearly inexpensive - Convenience of use - Simple structure	- Nozzle clogging - Low resolution - Low cell viability - Low-speed fabrication	[141,143–145]
Stereolithographic bioprinting			10^6	90		0.2–6	- Very high resolution - Removability of uncured resin from final products	- limited in the material used (photo-sensitive materials) - Unclear long-time effects due to DNA damage of UV exposure -Low speed	[124,146–149]
Laser-based bioprinting			10^8	95	Up to 300	50	-High resolution -High cell density -Free from nozzle clogging	- Costly - low scalability - Long-term harm caused by exposure to toxic particles and radiation - one bio-material at a time - Not related to ECM viscosity	[129,146–149]

printing, but a high number of hBMSCs remained alive after 14 days. Accordingly, the viscosity of the bioink varies for each type of cell, and the optimum amount should be investigated for different cells. WNF at any concentration could significantly enhance the rheological properties of the bioinks, making them more printable [160]. The advantage of extrusion bioprinting over inkjet bioprinting is the density of deposited cells, which is higher than that of inkjet bioprinting. On the other hand, due to shear stress and mechanical pressure occurring along with the dispensing procedure, the survival rate of cells may be lower as compared to inkjet bioprinting. Some countermeasures could be taken to boost cell survival rate, including lowering extrusion pressure and increasing nozzle size, resulting in compromised printing speed and quality [153,161]. Printing speed, layer height, the number of layers, flow rate, material viscosity, temperature, and needle diameter are important factors to have a defined and precise scaffold; they should be appropriately set in this method.

Currently, extrusion-based bioprinting is the most applicable method and much research has been performed on this technique. To create a bioactive 3D-bioprinted composite scaffold for bone tissue engineering, Kolan *et al*. used a PCL/13-93B3 glass composite as a structural material and pluronic hydrogel as supporting material for cells by using an extrusion bioprinter and studied the bioactivity and biodegradation rate of scaffolds. The formation of hydroxyapatite-like crystals on the scaffold surface proved the bioactivity of composite materials. Despite the unsteady nature of Pluronic hydrogel, microscopic images and weight loss demonstrated the presence of this hydrogel after one week of soaking in the culture media [162]. In another study on borate BGs, scaffolds made out of PLA and BG with different weight ratios (50, 33 %) by 3D bioprinting showed that adding borate BGs increased mechanical strength. Moreover, 3D bioprinting of PLA/borate BG paste and Alg/Gel hydrogel containing adipose-derived stem cells (ASCs) did not show uniform cell viability along the scaffolds; half bottom regions presented more dead cells, possibly due to the hypoxic condition with the lack of sufficient media and oxygen in downer parts [163]. Replacing PCL with PLA in the above-mentioned paste formula led to an increased brittleness by adding borate BG (50 % wt) to PCL. On the other hand, adding borate BG to PCL/Alg-Gel increased the mechanical strength of scaffolds. The cell viability showed the same results as the paste with PLA [164]. Murphy *et al.* investigated the effect of borate BG on scaffold bioactivity. They prepared a paste with PCL, 13-93B3 borate BG and matrigel containing ASCs to print a scaffold by using a 3D extrusion bioprinting. The results revealed that the release of BG ions during two weeks was more controllable than conventional melt deposition bioprinting. Hydroxyapatite-like crystals formed on the surface of the scaffold indicated the high bioactivity potential of scaffolds that makes them appropriate materials for bone tissue engineering [165].

By-products resulting from the degradation of Si-containing structures have been reported to cause a high level of osteoconductivity, but the cytotoxicity of these products should be assessed [166]. Wang *et al.* prepared a hydrogel of sodium alginate/gelatin containing polyphosphate Ca^{2+}-complex, silica, or borosilicate glasses; SaOS-2 cells were added to the hydrogel for bioprinting bone scaffolds. They assessed the effect of these materials on SaOS-2 cells. After 3 days of incubation, constructs containing polyphosphate Ca^{2+}-complex and biosilica

remarkably increased cell growth and proliferation. Biomineralization studies of incubation SaOS-2 cells embedded in different constructs for 3 days in the absence of an osteogenic cocktail and further 5 days in the presence of the cocktail showed that adding BGs promoted mineralization notably [167]. As stated earlier, MBGs are known for their high specific surface area and highly ordered mesoporous channel structure. These substances are proper for delivering various drugs and growth factors. In a previously performed study, a series of Zn-containing MBGs (0, 5, 10, or 15 mol% of Zn) were synthesized in which Zn partially or substituted Ca (15 mol%) for enhancing osteogenic and antimicrobial properties [168]. An alginate-methylcellulose blend containing up to 7 % Zn-containing MBGs was prepared while preserving rheological characteristics acceptable for the 3D printing of scaffolds with sufficient shape fidelity. These composites have been proven to be suitable for bioprinting with immortalized human mesenchymal stem cells. Composite scaffolds were found to absorb Ca and P (phosphorus) ions, while the released concentrations of Zn^{2+} matched the starting amount of this ion in produced glasses, implying that it can be regulated during the MBG synthesis stage. Reakasame *et al.* introduced 45S5 BG particles into alginate dialdehyde (ADA)-keratin microcapsules to improve biomineralization of the matrix and, thus, promote osteointegration in comparison to alginate- keratin and ADA-keratin microcapsules. Their outcomes revealed that adding BGs enhances the growth of calcium phosphate on the matrix surface in immersion in SBF. Besides, the cell viability of osteosarcoma cells encapsulated into all microcapsules increased during three weeks of cultivation [169]. In another study, ADA-Gel hydrogel + nano-scaled BG was prepared to investigate the survival rate of rat bone marrow-derived mesenchymal stem cells (rMSCs) *in vitro* and *in vivo*. The prepared scaffolds seemed to be capable of preserving rMSCs effectively *in vitro* and *in vivo* for a short period; however, a significant drop in survival rates was evident after 4 weeks. The *in vivo* implantation showed tissue integration and signs of biomaterial degradation (Fig. 8. a-d). The implants showed good biocompatibility and minimal immune reactions (Fig. 8. e-f). Angiogenesis and cell survival seemed to be positively impacted by nano-sized BGs. Angiogenesis was clearly induced by the implanted MSCs by attracting endothelial cells (Fig. 8. g-h) [170].

The third method for bioprinting is stereolithographic-based bioprinting. This is a nozzle-free process in which hydrogel precursors are crosslinked through photoirradiation [171]. Photocuring, the process of hardening the hydrogel, is done by adding photoinitiators. For fabricating a 3D construct, the bioink is put in a Petri dish to the desired layer height and then photocuring occurred according to the model image and CAM file (.stl). This process is repeated until all the patterned images are completed. After bioprinting, an uncrosslinked portion of bioink is removed and the desired 3D construct is obtained [172]. The resolution in this technique depends on the stereolithography approach; the multiphoton approach has a higher resolution than the single-photon. By this method, a resolution of 20 μm could be achieved [157].

Laser-based bioprinting is another method for bioprinting that uses a laser as a source of energy for curing bioinks. This method includes a pulsed laser source, a base structure or donor slide to support the printing material, and a receiving slide to collect the printed material [173]. For creating a 3D scaffold, a beam of a pulsed laser scans over a ribbon that is coated with a metallic absorbing layer (e.g., gold). The sacrificial absorbent layer vaporizes as a result of this process. Initially, the ensuing vapor bubbles would collapse on the absorbent layer surface without ejecting. Once the energy in the bubble builds up, the pressure inside the bubble rises until the bubble bursts and the bioink ejects onto the receiving substrate [161,174]. By this technique, excellent resolution (around 20 μm) and cell viability could be achieved [157]. The two last methods have not yet been applied to the bioprinting of BGs in tissue engineering.

5. Conclusions and future perspectives

The capability of prototyping complex and hierarchical structures with mass customization is the main advantage of 3D printing. Advances in nanotechnology and 3D printing have opened up new opportunities for bone tissue engineering. However, 3D printing approaches have still to face big challenges, including high cost and lower speed, creating space between the next layers, and creating additional porosity and limited materials suitable for 3D printing. Moreover, adding cells after printing a scaffold is random because cells will not distribute along the scaffold as desired. BGs can be used as additions to various base materials in 3D printed and 3D bioprinted bone scaffolds because of their unique physicochemical and mechanical qualities. When mixed with polymers, BGs can impart extra-functionalities to the final composite such as bioactivity, improved angiogenic and osteogenic properties, antibacterial effect, etc., which can contribute to accelerateìing tissue healing. 3D bioprinting has shown tremendous potential in bone tissue engineering. Despite many efforts to develop bioprinting techniques and studies in bioprinting, this technique has always been associated with challenges. Bioprinting for bone tissue engineering depends on chemical and physical factors to ensure proliferation, migration, osteogenesis, and angiogenesis. However, the bioprinting technique may overcome some of the obstacles by creating interconnected pores and surface topography required for bone tissue engineering. The inability to print small vessels, the lack of printable bioinks, the appropriate high-resolution bioprinting techniques, the complexity of the non-biological printing process, and the unstable cellular behavior are some of the challenges that bioprinting faces. One of the most important components of 3D bioprinting is the bioink which should be considered in priority for progress in building bone tissue and addressing existing challenges. Printed bone tissue must have good mechanical properties and functions and have a stable structure to meet the challenges of producing vascular bone tissue, but bioprinting is incapable of printing vessels in the size and scale of the vascular systems of the human body. It seems that extrusion-based bioprinting and droplet-based bioprinting techniques can compensate for the limitations of printing and create more diverse bioink formulations. It is also possible to create new compounds by adding suitable smart materials to bioink, as well as the use of decellularized extracellular matrix-based bioinks can provide promising results for bioprinting. Becoming vascular, maintaining cell viability, and cell migration are the main limiting factors in the production of bone tissue. Therefore, the development of an ideal bioink to meet the challenges of bioprinting is one of the most important factors to consider. The addition of nanoparticles, especially bioactive glasses to bioinks, can improve mechanical properties and increase cell viability and activity, cell differentiation, and proliferation. As a bioink, this compound plays a stimulating role in differentiating cells into bone cells and enhancing osteogenesis and angiogenesis. Finally, we believe that advances in bioprinting to create a complex structure of bone tissue along with vascular tissue will reach new heights soon.

CRediT authorship contribution statement

Sara Simorgh: Methodology, Investigation, Writing – original draft. **Neda Alasvand:** Methodology, Investigation, Writing – original draft. **Mahboobe Khodadadi:** Investigation, Resources, Writing – original draft. **Faezeh Ghobadi:** Formal analysis, Resources, Writing – original draft. **Maziar Malekzadeh Kebria:** Formal analysis, Resources. **Peiman Brouki Milan:** Writing – review & editing. **Saeid Kargozar:** Methodology, Writing – review & editing. **Francesco Baino:** Validation, Writing – review & editing. **Ali Mobasheri:** Validation, Writing – review & editing. **Masoud Mozafari:** Conceptualization, Writing – review & editing, Supervision, Project administration.

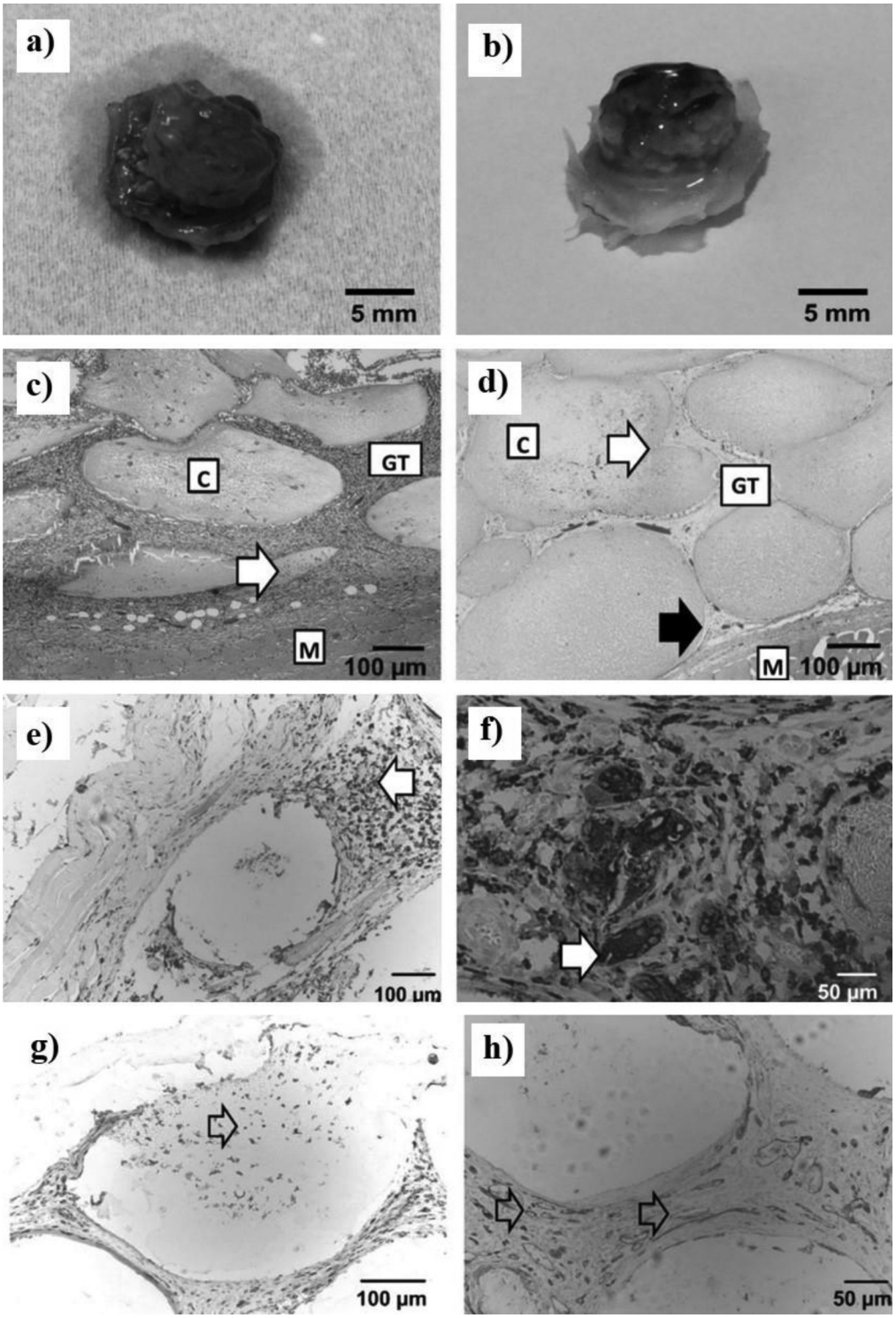

Fig. 8. (a-d) Representative images of the macroscopic and microscopic (H&E-stained) figure of structures following explanation (not all groups are shown, as the structures with and without nBG did not differ macroscopically). (a) Group 1W_ADA-GEL-rMSC-nBG: loosely adhering, moist, transparent hydrogel beads; (b) Group 4W_ADA-GEL-rMSC: firm, well adhering, opaque hydrogel beads; (c) H&E staining, 10×, group 1W_ADA-GEL-rMSC: loose, highly cellular granulation tissue in the spaces between beads, varying degrees of infiltration with tiny cells (arrow); (d) H&E staining, 10×, group 4W_ADA-GEL_rMSC; thin septae of connective tissue infiltrating the capsules (white arrow); a thin gap is visible among capsules and connective tissue (black arrow); GT = granulation tissue, C = capsules, M = muscle. (e&f) Representative pictures of ED1 (CD68) immunohistochemical staining after 4 weeks, 10× (e) and 20 × magnification (f), representative images (not all groups are depicted). The granulation tissue had a small number of ED1 positive cells (e; arrow). In single structures, just a few foreign body giant cells were found (f; arrow). In qualitative microscopic inspection, there were no differences between the groups with and without nBG. (g&h) Representative pictures of lectin immunohistochemical staining at 10× (g) and 20 × magnification (h) (not all groups are depicted). Lectin-positive cells are brown, while lectin-negative cells are blue (counterstained with hemalaun). (g) Lectin-positive cells were widely scattered in the connective tissue between beads after 1 week. A small percentage of the infiltrating cells showed lectin staining (arrow). (h) The connective tissue between the microbeads was substantially vascularized after 4 weeks (arrows). In qualitative microscopic inspection, there were no differences between the groups with and without nBG [170]. (For interpretation of the references to color in this figure legend, the reader is referred to the web version of this article.)

Declaration of Competing Interest

The authors declare that they have no known competing financial interests or personal relationships that could have appeared to influence the work reported in this paper.

Data availability

This is a review article. No unpublished data has been used.

References

[1] D.F. Williams, Challenges with the development of biomaterials for sustainable tissue engineering, Front. Bioeng. Biotechnol. 7 (2019), p. 127-127.
[2] F.J. O'Brien, Biomaterials & scaffolds for tissue engineering, Mater. Today 14 (3) (2011) 88–95.
[3] P. Zare, et al., Alginate sulfate-based hydrogel/nanofiber composite scaffold with controlled Kartogenin delivery for tissue engineering, Carbohydr. Polym. 266 (2021), 118123.
[4] N. Abbasi, et al., Porous scaffolds for bone regeneration, J. Sci.: Adv. Mater. Devices 5 (1) (2020) 1–9.
[5] G. Lutzweiler, A. Ndreu Halili, N. Engin Vrana, The Overview of porous, bioactive scaffolds as instructive biomaterials for tissue regeneration and their clinical translation, Pharmaceutics 12 (7) (2020).
[6] S. Bagheri, et al., Control of cellular adhesiveness in hyaluronic acid-based hydrogel through varying degrees of phenol moiety cross-linking, J. Biomed. Mater. Res. Part A 109 (5) (2021) 649–658.
[7] E. Dobrzyńska, et al., State of the art in additive manufacturing and its possible chemical and particle hazards—review, Indoor Air 31 (6) (2021) 1733–1758.
[8] G. Liu, et al., Additive manufacturing of structural materials, Mater. Sci. Eng.: R: Rep. 145 (2021), 100596.
[9] M.A. Sarabia-Vallejos, et al., Innovation in additive manufacturing using polymers: a survey on the technological and material developments, Polymers 14 (7) (2022).
[10] T.D. Ngo, et al., Additive manufacturing (3D printing): A review of materials, methods, applications and challenges, Compos. B Eng. 143 (2018) 172–196.
[11] S.C. Ligon, et al., Polymers for 3D Printing and Customized Additive Manufacturing, Chem. Rev. 117 (15) (2017) 10212–10290.
[12] K. Tappa, U. Jammalamadaka, Novel Biomaterials Used in Medical 3D Printing Techniques, J Funct Biomater 9 (1) (2018).
[13] P. Szymczyk-Ziółkowska, et al., A review of fabrication polymer scaffolds for biomedical applications using additive manufacturing techniques, Biocyber. Biomed. Eng. 40 (2) (2020) 624–638.
[14] A. Hivechi, et al., Cellulose nanocrystal effect on crystallization kinetics and biological properties of electrospun polycaprolactone, Mater. Sci. Eng., C 121 (2021), 111855.
[15] M.P. Nikolova, M.S. Chavali, Recent advances in biomaterials for 3D scaffolds: A review, Bioact. Mater. 4 (2019) 271–292.
[16] S. Kargozar, et al., "Hard" ceramics for "Soft" tissue engineering: Paradox or opportunity? Acta Biomater. 115 (2020) 1–28.
[17] S. Kargozar, et al., Copper-containing bioactive glasses and glass-ceramics: From tissue regeneration to cancer therapeutic strategies, Mater. Sci. Eng., C 121 (2021), 111741.
[18] S. Kargozar, et al., Synthesis and physico-chemical characterization of fluoride (F)- and silver (Ag)-substituted sol-gel mesoporous bioactive glasses, Biomedical Glasses 5 (1) (2019) 185–192.
[19] M. Arango-Ospina, A.R. Boccaccini, Chapter 4 - Bioactive glasses and ceramics for tissue engineering, in: A.R. Boccaccini, P.X. Ma, L. Liverani (Eds.), Tissue Engineering Using Ceramics and Polymers, third ed., Woodhead Publishing, 2022, pp. 111–178.
[20] S. Punj, J. Singh, K. Singh, Ceramic biomaterials: Properties, state of the art and future prospectives, Ceram. Int. 47 (20) (2021) 28059–28074.
[21] P. Chocholata, V. Kulda, V. Babuska, Fabrication of Scaffolds for bone-tissue regeneration, Materials (Basel, Switzerland) 12 (4) (2019) 568.
[22] S. Jain, et al., A review on mechanical and In-vitro studies of polymer reinforced bioactive glass-scaffolds and their fabrication techniques, Ceram. Int. 48 (5) (2022) 5908–5921.
[23] Y. Ding, et al., 3D printing polylactic acid polymer-bioactive glass loaded with bone cement for bone defect in weight-bearing area, Front. Bioeng. Biotechnol. (2022) 10.
[24] E. Schätzlein, et al., 3D-Printed PLA-Bioglass Scaffolds with Controllable Calcium Release and MSC Adhesion for Bone Tissue Engineering, Polymers (Basel) 14 (12) (2022).
[25] F. Hernandez-Tenorio, C. Giraldo-Estrada, Characterization and chemical modification of pullulan produced from a submerged culture of Aureobasidium pullulans ATCC 15233, Polym. Test. 114 (2022), 107686.
[26] L. Weng, et al., Binary doping of strontium and copper enhancing osteogenesis and angiogenesis of bioactive glass nanofibers while suppressing osteoclast activity, ACS Appl. Mater. Interfaces 9 (29) (2017) 24484–24496.
[27] L. Drago, M. Toscano, M. Bottagisio, Recent evidence on bioactive glass antimicrobial and antibiofilm activity: a mini-review, Materials 11 (2) (2018) 326.
[28] M.N. Rahaman, et al., Bioactive glass in tissue engineering, Acta Biomater. 7 (6) (2011) 2355–2373.
[29] J.S. Fernandes, et al., Multifunctional bioactive glass and glass-ceramic biomaterials with antibacterial properties for repair and regeneration of bone tissue, Acta Biomater. 59 (2017) 2–11.
[30] S. Kargozar, et al., Bioactive glasses entering the mainstream, Drug Discovery Today 23 (10) (2018) 1700–1704.
[31] Q. Fu, Bioactive glass scaffolds for bone tissue engineering, in: Biomedical, Therapeutic and Clinical Applications of Bioactive Glasses, Elsevier, 2019, pp. 417–442.
[32] N. Top, et al., Computer-aided design and additive manufacturing of bone scaffolds for tissue engineering: state of the art, J. Mater. Res. 36 (19) (2021) 3725–3745.
[33] A.A. El-Rashidy, et al., Regenerating bone with bioactive glass scaffolds: A review of in vivo studies in bone defect models, Acta Biomater. 62 (2017) 1–28.
[34] A.V. Do, et al., 3D printing of scaffolds for tissue regeneration applications, Adv. Healthcare Mater. 4 (12) (2015) 1742–1762.
[35] F. Baino, S. Fiorilli, C. Vitale-Brovarone, Bioactive glass-based materials with hierarchical porosity for medical applications: Review of recent advances, Acta Biomater. 42 (2016) 18–32.
[36] R. Gmeiner, et al., Additive manufacturing of bioactive glasses and silicate bioceramics, J. Ceram. Sci. Technol 6 (2) (2015) 75–86.
[37] S. Bose, S. Vahabzadeh, A. Bandyopadhyay, Bone tissue engineering using 3D printing, Mater. Today 16 (12) (2013) 496–504.
[38] S. Bose, et al., Influence of random and designed porosities on 3D printed tricalcium phosphate-bioactive glass scaffolds, Addit. Manuf. 40 (2021), 101895.
[39] C.-Y. Chi, et al., Preparation and in-vitro evaluation of Fe2O3-doped DP-bioglass in combination with 3D-printing and selective laser sintering process (3DP-SLS) for alveolar bone augmentation, Ceram. Int. 47 (9) (2021) 12725–12734.
[40] F. Baino, et al., Processing methods for making porous bioactive glass-based scaffolds—A state-of-the-art review, Int. J. Appl. Ceram. Technol. 16 (5) (2019) 1762–1796.
[41] J. Liu, et al., Fabrication and characterization of porous 45S5 glass scaffolds via direct selective laser sintering, Mater. Manuf. Processes 28 (6) (2013) 610–615.
[42] C. Gao, et al., Enhancement mechanisms of graphene in nano-58S bioactive glass scaffold: mechanical and biological performance, Sci. Rep. 4 (1) (2014) 4712.
[43] K.C.R. Kolan, et al., 3D-printed biomimetic bioactive glass Scaffolds for bone regeneration in rat calvarial defects, Internat. J. Bioprint. 6 (2) (2020), p. 274-274.
[44] F.P. Melchels, J. Feijen, D.W. Grijpma, A review on stereolithography and its applications in biomedical engineering, Biomaterials 31 (24) (2010) 6121–6130.
[45] A.P. Moreno Madrid, et al., Advances in additive manufacturing for bone tissue engineering scaffolds, Mater. Sci. Eng., C 100 (2019) 631–644.
[46] C.-J. Bae, et al., Ceramic Stereolithography: Additive Manufacturing for 3D Complex Ceramic Structures, J. Korean Ceram. Soc. 54 (6) (2017) 470–477.
[47] D.A. Komissarenko, et al., Rheological and Curing Behavior of Acrylate-Based Suspensions for the DLP 3D Printing of Complex Zirconia Parts, Materials 11 (12) (2018).
[48] L. Yuan, S. Ding, C. Wen, Additive manufacturing technology for porous metal implant applications and triple minimal surface structures: A review, Bioact. Mater. 4 (2019) 56–70.
[49] R. Gmeiner, et al., Stereolithographic ceramic manufacturing of high strength bioactive glass, Int. J. Appl. Ceram. Technol. 12 (1) (2015) 38–45.
[50] B. Thavornyutikarn, et al., Porous 45S5 Bioglass®-based scaffolds using stereolithography: Effect of partial pre-sintering on structural and mechanical properties of scaffolds, Mater. Sci. Eng., C 75 (2017) 1281–1288.
[51] Q. Chen, et al., Ceramic Stereolithography of Bioactive Glasses: Influence of Resin Composition on Curing Behavior and Green Body Properties, Biomedicines 10 (2) (2022).
[52] J.-H. Kang, et al., Mechanical properties and optical evaluation of scaffolds produced from 45S5 bioactive glass suspensions via stereolithography, Ceram. Int. 46 (2) (2020) 2481–2488.
[53] M.V. Varma, B. Kandasubramanian, S.M. Ibrahim, 3D printed scaffolds for biomedical applications, Mater. Chem. Phys. 255 (2020), 123642.
[54] J. Schmidt, et al., Digital light processing of wollastonite-diopside glass-ceramic complex structures, J. Eur. Ceram. Soc. 38 (13) (2018) 4580–4584.
[55] Y. Zeng, et al., 3D printing of hydroxyapatite scaffolds with good mechanical and biocompatible properties by digital light processing, J. Mater. Sci. 53 (2018) 6291–6301.
[56] P. Tesavibul, et al., Processing of 45S5 Bioglass® by lithography-based additive manufacturing, Mater. Lett. 74 (2012) 81–84.
[57] W.L. Ng, et al., Vat polymerization-based bioprinting-process, materials, applications and regulatory challenges, Biofabrication 12 (2) (2020), 022001.
[58] O. Santoliquido, P. Colombo, A. Ortona, Additive Manufacturing of ceramic components by Digital Light Processing: A comparison between the "bottom-up" and the "top-down" approaches, J. Eur. Ceram. Soc. 39 (6) (2019) 2140–2148.
[59] X. Li, et al., Fabrication of porous β-TCP/58S bioglass scaffolds via top-down DLP printing with high solid loading ceramic-resin slurry, Mater. Chem. Phys. 267 (2021), 124587.
[60] Cesarano, J., *A review of robocasting technology*. MRS Online Proceedings Library (OPL), 1998. **542**.
[61] S. Eqtesadi, et al., Robocasting of 45S5 bioactive glass scaffolds for bone tissue engineering, J. Eur. Ceram. Soc. 34 (1) (2014) 107–118.
[62] Q. Fu, et al., Bioactive glass scaffolds for bone tissue engineering: state of the art and future perspectives, Mater. Sci. Eng., C 31 (7) (2011) 1245–1256.

[63] G. Tarì, et al., Influence of particle size distribution on colloidal processing of alumina, J. Eur. Ceram. Soc. 18 (3) (1998) 249–253.

[64] S. Olhero, J. Ferreira, Influence of particle size distribution on rheology and particle packing of silica-based suspensions, Powder Technol. 139 (1) (2004) 69–75.

[65] Tarì, G., J.M. Ferreira, and A.T. Fonseca, *Influence of particle size and particle size distribution on drying-shrinkage behaviour of alumina slip cast bodies.* Ceramics International, 1999. **25**(6): p. 577-580.

[66] A. Kaushal, S.M. Olhero, J. Ferreira, Lead-free 0.5 Ba (Zr 0.2 Ti 0.8) O 3–0.5 (Ba 0.7 Ca 0.3) TiO 3 powder surface treated against hydrolysis–a key for a successful aqueous processing, J. Mater. Chem. C 1 (32) (2013) 4846–4853.

[67] J.V. Milewski, Efficient use of whiskers in the reinforcement of ceramics, Advanced Ceramic Materials 1 (1986) 36–41.

[68] X. Liu, M.N. Rahaman, Q. Fu, Bone regeneration in strong porous bioactive glass (13–93) scaffolds with an oriented microstructure implanted in rat calvarial defects, Acta Biomater. 9 (1) (2013) 4889–4898.

[69] J. Barberi, et al., Robocasting of SiO2-based bioactive glass scaffolds with porosity gradient for bone regeneration and potential load-bearing applications, Materials 12 (17) (2019) 2691.

[70] K. Dixit, N. Sinha, Additive manufacturing of carbon nanotube reinforced bioactive glass scaffolds for bone tissue engineering, J. Eng. Sci. Med. Diagnost. Therapy 4 (4) (2021).

[71] L. Zhang, et al., Three-dimensional (3D) printed scaffold and material selection for bone repair, Acta Biomater. 84 (2019) 16–33.

[72] L.C. Hwa, et al., Recent advances in 3D printing of porous ceramics: A review, Curr. Opin. Solid State Mater. Sci. 21 (6) (2017) 323–347.

[73] X. Du, S. Fu, Y. Zhu, 3D printing of ceramic-based scaffolds for bone tissue engineering: an overview, J. Mater. Chem. B 6 (27) (2018) 4397–4412.

[74] Kafle, A., et al., *3D/4D Printing of Polymers: Fused Deposition Modelling (FDM), Selective Laser Sintering (SLS), and Stereolithography (SLA).* Polymers, 2021. **13** (18).

[75] F. Baino, E. Verné, J. Massera, Additive manufacturing of bioactive glasses, J. 3D Print. Med. 2 (2) (2018) 47–49.

[76] M.H. Monfared, et al., Preparation and characterization of 3D nanocomposite scaffold from bioactive glass/β-tricalcium phosphate via Robocasting method for bone tissue engineering, J. Non-Cryst. Solids 593 (2022), 121769.

[77] A. Dukle, et al., Can 3D-Printed Bioactive Glasses Be the Future of Bone Tissue Engineering? Polymers (Basel) 14 (8) (2022).

[78] Y. Zhou, W. Grayson, Three-dimensional printing of scaffolds for facial reconstruction, MRS Bull. (2022) 1–7.

[79] J.A. Lewis, Direct ink writing of 3D functional materials, Adv. Funct. Mater. 16 (17) (2006) 2193–2204.

[80] J. Li, et al., 3D printing of hydrogels: Rational design strategies and emerging biomedical applications, Mater. Sci. Eng.: R: Rep. 140 (2020), 100543.

[81] G. Dong, et al., Optimizing process parameters of fused deposition modeling by Taguchi method for the fabrication of lattice structures, Addit. Manuf. 19 (2018) 62–72.

[82] O.S. Carneiro, A. Silva, R. Gomes, Fused deposition modeling with polypropylene, Mater. Des. 83 (2015) 768–776.

[83] A.M. Arefin, et al., Polymer 3D printing review: Materials, process, and design strategies for medical applications, Polymers 13 (9) (2021) 1499.

[84] J. Butt, R. Bhaskar, Investigating the effects of annealing on the mechanical properties of FFF-printed thermoplastics, J. Manuf. Mater. Process. 4 (2) (2020) 38.

[85] E.N. Peters, Plastics: thermoplastics, thermosets, and elastomers, Wiley-Interscience, New York, 2002.

[86] A. Fathi, et al., Three-dimensionally printed polycaprolactone/multicomponent bioactive glass scaffolds for potential application in bone tissue engineering, Biomedical Glasses 6 (1) (2020) 57–69.

[87] I.T. Ozbolat, M. Hospodiuk, Current advances and future perspectives in extrusion-based bioprinting, Biomaterials 76 (2016) 321–343.

[88] E. Zeimaran, et al., Advances in bioactive glass-containing injectable hydrogel biomaterials for tissue regeneration, Acta Biomater. 136 (2021) 1–36.

[89] A. Shapira, et al., Stabilization strategies in extrusion-based 3D bioprinting for tissue engineering, Appl. Phys. Rev. 5 (4) (2018), 041112.

[90] H. Yuk, et al., Hydraulic hydrogel actuators and robots optically and sonically camouflaged in water, Nat. Commun. 8 (1) (2017) 1–12.

[91] R. Landers, et al., Fabrication of soft tissue engineering scaffolds by means of rapid prototyping techniques, J. Mater. Sci. 37 (15) (2002) 3107–3116.

[92] R. Landers, et al., Rapid prototyping of scaffolds derived from thermoreversible hydrogels and tailored for applications in tissue engineering, Biomaterials 23 (23) (2002) 4437–4447.

[93] A. Skardal, et al., Photocrosslinkable hyaluronan-gelatin hydrogels for two-step bioprinting, Tissue Eng. Part A 16 (8) (2010) 2675–2685.

[94] Fancy, D.A. and T. Kodadek, *Chemistry for the analysis of protein–protein interactions: rapid and efficient cross-linking triggered by long wavelength light.* Proceedings of the National Academy of Sciences, 1999. **96**(11): p. 6020-6024.

[95] E. Axpe, M.L. Oyen, Applications of alginate-based bioinks in 3D bioprinting, Int. J. Mol. Sci. 17 (12) (2016) 1976.

[96] T. Xu, et al., Fabrication and characterization of bio-engineered cardiac pseudo tissues, Biofabrication 1 (3) (2009), 035001.

[97] P.S. Gungor-Ozkerim, et al., Bioinks for 3D bioprinting: an overview, Biomater. Sci. 6 (5) (2018) 915–946.

[98] T.H. Jovic, et al., Plant-derived biomaterials: A review of 3D bioprinting and biomedical applications, Front. Mech. Eng. 5 (2019) 19.

[99] Q. Zeng, et al., Bioglass/alginate composite hydrogel beads as cell carriers for bone regeneration, J. Biomed. Mater. Res. B Appl. Biomater. 102 (1) (2014) 42–51.

[100] J. Wu, et al., 3D printing mesoporous bioactive glass/sodium alginate/gelatin sustained release scaffolds for bone repair, J. Biomater. Appl. 33 (6) (2019) 755–765.

[101] G. Luo, et al., 13–93 bioactive glass/alginate composite scaffolds 3D printed under mild conditions for bone regeneration, RSC Adv. 7 (20) (2017) 11880–11889.

[102] Y. Zhang, et al., Recent advances in 3D bioprinting of vascularized tissues, Mater. Des. (2020), 109398.

[103] M.C. Gómez-Guillén, et al., Structural and physical properties of gelatin extracted from different marine species: a comparative study, Food Hydrocolloids 16 (1) (2002) 25–34.

[104] M. Bertuola, et al., Gelatin–alginate–hyaluronic acid inks for 3D printing: effects of bioglass addition on printability, rheology and scaffold tensile modulus, J. Mater. Sci. (2021) 1–17.

[105] S. Rhee, et al., 3D bioprinting of spatially heterogeneous collagen constructs for cartilage tissue engineering, ACS Biomater. Sci. Eng. 2 (10) (2016) 1800–1805.

[106] B. Sarker, et al., Combining collagen and bioactive glasses for bone tissue engineering: a review, Adv. Healthcare Mater. 4 (2) (2015) 176–194.

[107] N.S. Kajave, et al., Bioglass incorporated methacrylated collagen bioactive ink for 3D printing of bone tissue, Biomed. Mater. 16 (3) (2021), 035003.

[108] K. Schuhladen, et al., The effect of borate bioactive glass on the printability of methylcellulose-manuka honey hydrogels, J. Mater. Res. (2021) 1–8.

[109] T. Distler, et al., Polymer-bioactive glass composite filaments for 3D Scaffold manufacturing by fused deposition modeling: fabrication and characterization, Front. Bioeng. Biotechnol. 8 (552) (2020).

[110] R. Govender, et al., Polymers in pharmaceutical additive manufacturing: A balancing act between printability and product performance, Adv. Drug Deliv. Rev. 177 (2021), 113923.

[111] B.N. Turner, R. Strong, S.A. Gold, A review of melt extrusion additive manufacturing processes: I. Process design and modeling, Rapid Prototyp. J. (2014).

[112] Y. Kim, et al., 3D-printed PCL/bioglass (BGS-7) composite scaffolds with high toughness and cell-responses for bone tissue regeneration, J. Ind. Eng. Chem. 79 (2019) 163–171.

[113] S.-L. Bee, et al., Approaches to improve therapeutic efficacy of biodegradable PLA/PLGA microspheres: a review, Polym. Rev. 58 (3) (2018) 495–536.

[114] Y. Cheng, et al., Polylactic acid (PLA) synthesis and modifications: a review, Front. Chem. China 4 (3) (2009) 259–264.

[115] S.A.M. Estrada, et al., Evaluation of in vitro bioactivity of 45S5 bioactive glass/poly lactic acid scaffolds produced by 3D printing, Int. J. Compos. Mater 7 (5) (2017) 144–149.

[116] P. Pei, et al., Three-dimensional printing of tricalcium silicate/mesoporous bioactive glass cement scaffolds for bone regeneration, J. Mater. Chem. B 4 (46) (2016) 7452–7463.

[117] J. Lim, et al., Emerging bone tissue engineering via Polyhydroxyalkanoate (PHA)-based scaffolds, Mater. Sci. Eng., C 79 (2017) 917–929.

[118] C. Romagnoli, F. D'Asta, M.L. Brandi, Drug delivery using composite scaffolds in the context of bone tissue engineering, Clin. Cases Mineral Bone Metab. 10 (3) (2013) 155–161.

[119] X. Du, et al., 3D printing of mesoporous bioactive glass/silk fibroin composite scaffolds for bone tissue engineering, Mater. Sci. Eng., C 103 (2019), 109731.

[120] P. Pei, Z. Tian, Y. Zhu, 3D printed mesoporous bioactive glass/metal-organic framework scaffolds with antitubercular drug delivery, Microporous Mesoporous Mater. 272 (2018) 24–30.

[121] A.B. Touré, E. Mele, J.K. Christie, Multi-layer scaffolds of poly (Caprolactone), poly (glycerol sebacate) and bioactive glasses manufactured by combined 3d printing and electrospinning, Nanomaterials 10 (4) (2020) 626.

[122] E. Daskalakis, et al., Novel 3D bioglass scaffolds for bone tissue regeneration, Polymers 14 (3) (2022) 445.

[123] Y. Zhang, et al., Mesoporous bioactive glass nanolayer-functionalized 3D-printed scaffolds for accelerating osteogenesis and angiogenesis, Nanoscale 7 (45) (2015) 19207–19221.

[124] S. Agarwal, et al., *Current Developments in 3D Bioprinting for Tissue and Organ Regeneration–A Review.* Frontiers, Mechanical Engineering 6 (90) (2020).

[125] P. Datta, et al., Essential steps in bioprinting: From pre- to post-bioprinting, Biotechnol. Adv. 36 (5) (2018) 1481–1504.

[126] Iordache, F., *Chapter 2 - Bioprinted scaffolds*, in *Materials for Biomedical Engineering*, A.-M. Holban and A.M. Grumezescu, Editors. 2019, Elsevier. p. 35-60.

[127] J. Groll, et al., A definition of bioinks and their distinction from biomaterial inks, Biofabrication 11 (1) (2018), 013001.

[128] J. Gopinathan, I. Noh, Recent trends in bioinks for 3D printing, Biomater. Res. 22 (1) (2018) 1–15.

[129] Z. Gu, et al., Development of 3D bioprinting: From printing methods to biomedical applications, Asian J. Pharm. Sci. 15 (5) (2020) 529–557.

[130] I.T. Ozbolat, Scaffold-based or Scaffold-free bioprinting: competing or complementing approaches? J. Nanotechnol. Eng. Med. 6 (2) (2015).

[131] Z. Wang, et al., Tissue-specific engineering: 3D bioprinting in regenerative medicine, J. Control. Release 329 (2021) 237–256.

[132] G. Cidonio, et al., Printing bone in a gel: using nanocomposite bioink to print functionalised bone scaffolds, Materials Today Bio 4 (2019), 100028.

[133] M. Wang, L. Guo, H. Sun, Manufacture of biomaterials, in: R. Narayan (Ed.), Encyclopedia of Biomedical Engineering, Elsevier, Oxford, 2019, pp. 116–134.

[134] M. Hospodiuk, et al., The bioink: A comprehensive review on bioprintable materials, Biotechnol. Adv. 35 (2) (2017) 217–239.
[135] S. Choi, H. Ahn, S.-H. Kim, Tyrosinase-mediated hydrogel crosslinking for tissue engineering, J. Appl. Polym. Sci. 139 (14) (2022) 51887.
[136] S. Khoee, A. Sadeghi, An NIR-triggered drug release and highly efficient photodynamic therapy from PCL/PNIPAm/porphyrin modified graphene oxide nanoparticles with the Janus morphology, RSC Adv. (2019).
[137] T. Ni, et al., 3D bioprinting of bone marrow mesenchymal stem cell-laden silk fibroin double network scaffolds for cartilage tissue repair, Bioconjug. Chem. 31 (8) (2020) 1938–1947.
[138] G.L. Koons, M. Diba, A.G. Mikos, Materials design for bone-tissue engineering, Nat. Rev. Mater. 5 (8) (2020) 584–603.
[139] B. Yilmaz, et al., Bioprinting: A review of processes, materials and applications, Bioprinting 23 (2021) e00148.
[140] B.P. Oropeza, et al., Assessment of angiogenesis and cell survivability of an inkjet bioprinted biological implant in an animal model, Materials (Basel) 15 (13) (2022).
[141] Y. Cai, et al., Nanocomposite bioinks for 3D bioprinting, Acta Biomater. (2022).
[142] X. Li, et al., Inkjet bioprinting of biomaterials, Chem. Rev. 120 (19) (2020) 10793–10833.
[143] S. Vijayavenkataraman, et al., 3D bioprinting of tissues and organs for regenerative medicine, Adv. Drug Deliv. Rev. 132 (2018) 296–332.
[144] N. Betancourt, X. Chen, Review of extrusion-based multi-material bioprinting processes, Bioprinting 25 (2022) e00189.
[145] L. Ning, X. Chen, A brief review of extrusion-based tissue scaffold bio-printing, Biotechnol. J. 12 (8) (2017).
[146] M. Mobaraki, et al., Bioinks and bioprinting: A focused review, Bioprinting 18 (2020) e00080.
[147] A. Fatimi, et al., Natural Hydrogel-Based Bio-Inks for 3D Bioprinting in Tissue Engineering, *A Review.* Gels 8 (3) (2022).
[148] Yu, J., et al., Current Advances in 3D Bioprinting Technology and Its Applications for Tissue Engineering. Polymers (Basel), 2020. **12**(12).
[149] E.S. Bishop, et al., 3-D bioprinting technologies in tissue engineering and regenerative medicine: Current and future trends, Genes & Diseases 4 (4) (2017) 185–195.
[150] S. Derakhshanfar, et al., 3D bioprinting for biomedical devices and tissue engineering: A review of recent trends and advances, Bioact. Mater. 3 (2) (2018) 144–156.
[151] X. Cui, et al., Thermal inkjet printing in tissue engineering and regenerative medicine, Recent Pat. Drug Delivery Formulation 6 (2) (2012) 149–155.
[152] G. Turnbull, et al., 3D bioactive composite scaffolds for bone tissue engineering, Bioact. Mater. 3 (3) (2018) 278–314.
[153] M. Salah, et al., Three-dimensional bio-printing and bone tissue engineering: technical innovations and potential applications in maxillofacial reconstructive surgery, Maxillofacial Plastic and Reconstructive Surgery 42 (1) (2020) 18.
[154] S. Iwanaga, K. Arai, M. Nakamura, Chapter 4 - Inkjet Bioprinting, in: A. Atala, J. J. Yoo (Eds.), Essentials of 3D Biofabrication and Translation, Academic Press, Boston, 2015, pp. 61–79.
[155] G. Gao, et al., Bioactive nanoparticles stimulate bone tissue formation in bioprinted three-dimensional scaffold and human mesenchymal stem cells, Biotechnol. J. 9 (10) (2014) 1304–1311.
[156] Pati, F., et al. *Chapter 7 Extrusion Bioprinting.* 2015.
[157] Rider, P., et al., *Bioprinting of tissue engineering scaffolds.* Journal of tissue engineering, 2018. **9**: p. 2041731418802090-2041731418802090.
[158] M. Shin, et al., Gallol-derived ECM-mimetic adhesive bioinks exhibiting temporal shear-thinning and stabilization behavior, Acta Biomater. 95 (2019) 165–175.
[159] K. Hölzl, et al., Bioink properties before, during and after 3D bioprinting, Biofabrication 8 (3) (2016), 032002.
[160] M. Ojansivu, et al., Wood-based nanocellulose and bioactive glass modified gelatin-alginate bioinks for 3D bioprinting of bone cells, Biofabrication 11 (3) (2019), 035010.
[161] N. Li, R. Guo, Z.J. Zhang, Bioink Formulations for Bone Tissue Regeneration, Front. Bioeng. Biotechnol. (2021) 9.
[162] K. Kolan, et al., Solvent Based 3D Printing of Biopolymer/Bioactive Glass Composite and Hydrogel for Tissue Engineering Applications, Procedia CIRP 65 (2017) 38–43.
[163] K.C.R. Kolan, et al., Bioprinting with bioactive glass loaded polylactic acid composite and human adipose stem cells, Bioprinting 18 (2020) e00075.
[164] K.C.R. Kolan, et al., Bioprinting with human stem cell-laden alginate-gelatin bioink and bioactive glass for tissue engineering, Internat. J. Bioprint. 5 (2.2) (2019), 204-204.
[165] C. Murphy, et al., 3D bioprinting of stem cells and polymer/bioactive glass composite scaffolds for bone tissue engineering, Internat. J. Bioprint. 3 (1) (2017), 005-005.
[166] S. Heid, A.R. Boccaccini, Advancing bioinks for 3D bioprinting using reactive fillers: A review, Acta Biomater. 113 (2020) 1–22.
[167] X. Wang, et al., Effect of Bioglass on Growth and Biomineralization of SaOS-2 Cells in Hydrogel after 3D Cell Bioprinting, PLoS ONE 9 (11) (2014) e112497.
[168] V. Guduric, et al., Tailorable Zinc-Substituted Mesoporous Bioactive Glass/Alginate-Methylcellulose Composite Bioinks, Materials 14 (5) (2021) 1225.
[169] S. Reakasame, et al., Cell laden alginate-keratin based composite microcapsules containing bioactive glass for tissue engineering applications, J. Mater. Sci. - Mater. Med. (2018) 29.
[170] U. Rottensteiner-Brandl, et al., Encapsulation of Rat Bone Marrow Derived Mesenchymal Stem Cells in Alginate Dialdehyde/Gelatin Microbeads with and without Nanoscaled Bioactive Glass for In Vivo Bone Tissue Engineering, Materials (Basel) 11 (10) (2018).
[171] R. Raman, R. Bashir, Chapter 6 - Stereolithographic 3D Bioprinting for Biomedical Applications, in: A. Atala, J.J. Yoo (Eds.), Essentials of 3D Biofabrication and Translation, Academic Press, Boston, 2015, pp. 89–121.
[172] H. Kumar, K. Kim, Stereolithography 3D Bioprinting, Methods Mol. Biol. 2140 (2020) 93–108.
[173] D.M. Kingsley, et al., Laser-based 3D bioprinting for spatial and size control of tumor spheroids and embryoid bodies, Acta Biomater. 95 (2019) 357–370.
[174] D. Hakobyan, et al., Laser-Assisted Bioprinting for Bone Repair, Methods Mol. Biol. 2140 (2020) 135–144.